

Identification and mechanistic Studies of novel preclinical Co-potentiator for CFTR  
gating Mutations

by

Houriyeh Hajizadeh

Graduate Department of Physiology

McGill University, Montreal

November 2023

A thesis submitted to McGill University in partial fulfilment of the requirements for the degree of

Master of Science

First published on 11 December 2024

© Houriyeh Hajizadeh 2024

## Abstract

Cystic fibrosis (CF) is one of the most common life-threatening genetic diseases. More than ~105,000 people are estimated to have been diagnosed with CF worldwide, primarily affecting their respiratory and digestive systems. CF transmembrane conductance regulator (CFTR) is an ATP-gated anion-selective channel with >2000 mutations. The third most common mutation, G551D, results in a gating defect and profoundly reduces the open probability ( $P_o$ ) than its wild-type counterpart (WT-CFTR). Ivacaftor (VX-770), an FDA-approved drug, which acts as a gating potentiator, can partially restore the G551D-CFTR channel activity. Elexacaftor (VX-445), together with the folding corrector tezacaftor (VX-661), and VX-770 are part of the recently approved modulator drug Trikafta combination. VX-445 is not only a corrector but also acts synergistically with VX-770 as a potentiator on the most common F508del and other mutants with both folding and gating defects. Remarkably, many rare CF mutations are poorly susceptible to the approved CFTR-modulator therapies. Thus, there is an unmet need to assess whether the activity of these mutants can be improved by preclinical potentiators.

Our laboratory has recently identified a new CFTR corrector molecule, 4172, which also displayed some gating potentiator activity. I hypothesized that 4172 and its analogs may have a distinct mechanism of action (MOA) from that of the VX-770 (class I) and VX-445 (class III) potentiators, with distinct binding sites in CFTR. Using fluorescence and electrophysiological transport assays I have shown that a panel of newly synthesized 4172 structural analogs belong to the “class II” potentiators, based on their additive effect with class I and III potentiators on polarized airway epithelial cells. These new class II potentiators display superior potency as compared to known class II potentiators with poor potency and bioavailability (apigenin and bis-DMC). Mechanistic studies revealed that CFTR channel activation by potentiator combination can be accomplished via PKA- and NBD1/2 dimerization-independent or non-canonical mechanisms.

## Résumé

La fibrose kystique (FK) est l'une des maladies génétiques mortelles les plus courantes. On estime que plus de 105 000 personnes dans le monde ont été diagnostiquées avec la FK, qui affecte principalement les systèmes respiratoire et digestif. Le régulateur de conductance transmembranaire de la fibrose kystique (CFTR) est un canal sélectif de l'ions chlorure, géré par l'ATP, qui présente plus de 2000 mutations. La troisième mutation la plus fréquente, G551D, entraîne un défaut de passage ionique et réduit considérablement la probabilité d'ouverture ( $P_o$ ) par rapport à son homologue de type sauvage (WT-CFTR). L'ivacaftor (VX-770), un médicament approuvé par la FDA, qui agit comme un potentialisateur de gating, peut restaurer partiellement l'activité du canal G551D-CFTR. L'elxacaftor (VX-445), le correcteur de repliement tezacaftor (VX-661) et le VX-770 font partie de l'association de médicaments modulateurs Trikafta, récemment approuvée par la FDA. Le VX-445 n'est pas seulement un correcteur, il agit également en synergie avec le VX-770 en tant que potentialisateur du F508del, la mutation la plus courante et sur d'autres mutants présentant des défauts de repliement et de gating. Il est remarquable que de nombreuses mutations rares de la fibrose kystique soient peu sensibles aux thérapies modulatrices de la CFTR approuvées. Il existe donc un besoin non satisfait d'évaluer si l'activité de ces mutants peut être améliorée par des potentialisateurs précliniques.

Notre laboratoire a récemment identifié une nouvelle molécule correctrice de la CFTR, la 4172, qui présentait également une certaine activité potentialisatrice de gating. J'ai émis l'hypothèse que le 4172 et ses analogues pourraient avoir un mécanisme d'action distinct de celui des potentialisateurs VX-770 (classe I) et VX-445 (classe III), avec des sites de liaison distincts dans la CFTR. En utilisant des essais de transport par fluorescence et électrophysiologiques, j'ai montré qu'un panel d'analogues structurels du 4172 nouvellement synthétisé appartient aux potentialisateurs de "classe II", sur la base de leur effet additif avec les potentialisateurs de classe I et III sur les cellules épithéliales polarisées des voies respiratoires. Ces nouveaux potentialisateurs de classe II présentent une puissance supérieure à celle des potentialisateurs de classe II connus dont la puissance et la biodisponibilité sont médiocres (apigénine et bis-DMC). Nos études mécanistiques ont révélé que l'activation du canal CFTR par la combinaison de potentiateurs peut être réalisée par des mécanismes indépendants de la PKA et de la dimérisation NBD1/2 ou par des mécanismes non canoniques.

## **Acknowledgements**

Words cannot express my gratitude to my professor, Dr. Gergely Lukacs, and my supervisory committee for their invaluable patience and feedback. I also could not have undertaken this journey without Dr. Guido Veit and Ms. Haijin Xu, who introduced me to methodologies applied and generously provided their expertise during my graduate studies. I am also grateful to my lab mates, for their experimental help, inspiration, and moral support.

I would be remiss in not mentioning my parents Roya and Kamal, my brother MJ, and my friends. Their love and belief in me have kept my spirits and motivation high during this journey. Lastly, getting through the long and difficult process of writing and completing my thesis would not have been possible without the unconditional care and support of my best friend Amin.

## **Author Contributions**

The overall design of the study was planned jointly by Houriyeh Hajizadeh, Drs. Guido Veit and Gergely Lukacs. Most of the experiments were performed and analyzed by Houriyeh Hajizadeh. Results described in Figures 4.3 (with Dr. C. Vaccarin), 4.4, 4.8, and 4.11C-D were obtained by Dr. G. Veit. Dr. G. Marzaro's group synthesized and provided the 4172 analogs. The thesis was written by Houriyeh Hajizadeh with feedback from Drs. G. Veit and G. Lukacs.

## Table of Contents

Abstract.....	ii
Résumé.....	iii
Acknowledgements.....	iv
Author contributions.....	iv
Table of Contents.....	v
List of Tables.....	viii
List of Figures.....	ix
Abbreviations.....	xi
<b>Chapter 1: Introduction.....</b>	<b>1</b>
1.1 Cystic fibrosis.....	2
1.1.1 History of Cystic Fibrosis.....	2
1.1.2 Cystic fibrosis clinical phenotype.....	3
1.1.3 Lung pathophysiology of CF.....	3
1.2 The CFTR structure.....	5
1.3 Classifications of CFTR mutations.....	5
1.4 CFTR function (activation, mechanism, and gating cycles).....	8
1.5 CFTR pharmacotherapy FDA-approved and investigational modulators.....	9
1.5.1. CFTR potentiators.....	9
1.5.2. CFTR correctors.....	10
1.5.3 The cAMP-elevating agent and inhibitors.....	12
1.6 CFTR gating mutations, mechanism, and mechanism of rescue theories.....	13
<b>Chapter 2: Rationale, and Hypothesis.....</b>	<b>23</b>

<b>Chapter 3: Materials and Methods</b> .....	25
3.1 CFTR modulators and antibodies.....	26
3.2 Cell lines and Tissue culture.....	26
3.2.1 Human bronchial epithelia (CFBE41o-) and inducible variants.....	26
3.2.2 Human bronchial epithelia (16HBE14o-), gene-edited variants.....	27
3.2.3 Human nasal epithelial (HNE) primary cells.....	28
3.3 Immunoblotting and protein analysis.....	28
3.4 Functional assays to detect CFTR.....	29
3.4.1 Short-circuit current ( $I_{sc}$ ) measurements.....	29
3.4.2 CFTR activity measurements by the halide-sensitive yellow fluorescent protein (YFP) assay.....	31
3.5 Statistical analysis.....	31
<b>Chapter 4: Results</b> .....	36
4.1 Identification of novel co-potentiators of CFTR gating mutants with improved potency and efficacy.....	37
4.1.1 Screening of the 4172 analogs for G551D-CFTR and N1303K-CFTR co-potentiator activity in CFBE41o- cells.....	37
4.1.2 Characterization of the best co-potentiators in the presence of FDA-approved potentiators VX-770 or VX-445.....	39
4.1.3 Evidence to support 4172 analogs as class II potentiators.....	40
4.1.4 Potency and efficacy of VX-770, VX-445 and 4172 analog-mediated triple potentiation of G551D-CFTR.....	41
4.1.5 Functional correction of N1303K-CFTR by triple potentiators in 16HBE14o- and primary primary human nasal epithelia (HNE) cells.....	42

4.1.6 The addition of a third potentiator increases the functional correction efficacy of some rare CF mutants.....	43
4.2 Mechanistic understanding of novel potentiators.....	44
4.2.1 The impact of VX-661 on the efficacy and potency of the 4172 analog potentiators...	44
4.2.2 Does the co-potentiator activity require CFTR phosphorylation?.....	45
4.2.3 Is NBD-dimerization required for CFTR variant activation by double or triple potentiation?.....	46
<b>Chapter 5: Discussion.....</b>	<b>62</b>
5.1 Characterization of Novel co-potentiators of CFTR gating Mutants as single, double, or triple potentiation.....	63
5.2 Towards mechanistic understanding of novel potentiators.....	67
<b>References.....</b>	<b>70</b>
<b>Appendices.....</b>	<b>78</b>

## List of Tables

Table 3.1. Krebs-bicarbonate solution for Ussing chamber.....	30
Table 4.1. Summary of all hit compounds' efficacy and potency.....	55

## List of Figures

Figure 1.1. Organs affected by cystic fibrosis (CF).....	15
Figure 1.2. Relationship between CFTR protein and lung pathophysiology of CF.....	15
Figure 1.3. Topology and CryoEm structure of the CFTR.....	16
Figure 1.4. Classification of CFTR mutations depicting fundamental molecular defects.....	17
Figure 1.5. Activation of CFTR channel.....	18
Figure 1.6. CFTR pharmacotherapy FDA-approved and investigational modulator.....	19
Figure 1.7. Chemical structures of CFTR modulators are commonly used.....	20
Figure 1.8. Location of the most prevalent single-point <i>CFTR</i> variants mapped onto the CFTR structure.....	20
Figure 1.9. Combinatorial profiling to classify potentiator mechanisms of action based on their additive activation of CFTR gating mutants.....	21
Figure 1.10. Binding sites of VX-770 (purple), VX-661 (orange), and VX-445 (yellow) in CFTR structure.....	22
Figure 1.11. Pharmacological rescue of folding and gating mutations.....	22
Figure 3.1. CFTR short-circuit current recording on cultured CFBE41o- monolayer in Ussing chamber.....	33
Figure 3.2. Activation of the WT-CFTR channel.....	34
Figure 3.3. The halide-sensitive Yellow Fluorescence Protein (YFP) quenching assay to measure CFTR-dependent chloride transport activity in the medium-throughput screening assay.....	35
Figure 4.1. Characterization of 4172 analogs as co-potentiators of the phosphorylated CFTR variants by the halide-sensitive fluorescence quenching assay in CFBE41o- cells..	48
Figure 4.2. Phosphorylated G551D-CFTR co-potentialiation by 4172 analogues in the presence of VX-445 or VX-770.....	49

Figure 4.3. Functional classification of the K0 series 4172 analogs potentiator activity based on their combinatorial cluster analysis using established class I-III potentiators and G551D-CFTR and halide-sensitive YFP expressing in CFBE41o- cells.....	50
Figure 4.4. The combination of three classes of potentiators leads to G551D-CFTR hyperactivation relative to the WT-CFTR.....	51
Figure 4.5. The combination of multiple potentiators leads to the activation of G551D.....	52
Figure 4.6. Not only the efficacy but the potency of the K052X (class II) increased by class I and III potentiators in G551D-CFTR expressing CFBE41o- cells.....	53
Figure 4.7. The efficacy and potency of 4172 analogues on the phosphorylated N1303K-CFTR activity in the presence of VX-770 and VX-445.....	54
Figure 4.8. Correction efficacy of triple potentiator combinations on N1303K-CFTR in primary HNE epithelia.....	56
Figure 4.9. The 4172 co-potentiator analogs augment the phosphorylated S549R-CFTR mutant activity in CFBE41o- cells, determined by the halide-sensitive YFP assay.....	57
Figure 4.10. Effect of VX-661 corrector on the potency of the K064X, K070X, and K052X potentiators on N1303K- and S549R-CFTR activity in 16HBE14o- and CFBE cells respectively, in the presence of the VX-770 and VX-445.....	58
Figure 4.11. Triple potentiator-mediated 15SA-CFTR activation does not require the CFTR R domain phosphorylation in CFBE41o- and 16HBEo- cells.....	59
Figure 4.12. Phosphorylation independency of K series compound on CFTR potentiation.....	60
Figure 4.13. Triple potentiator-mediated CFTR activation is independent of NBD-dimerization...	61
Figure S.1. The CFTR expression of WT-, G551D-, and N1303K-, S549R-, S549N- and W1282X-CFTR.....	79
Figure S.2. The combination of multiple potentiators does not lead to activation of S549N-CFTR/YFP.....	80

## Abbreviations

a.u.	arbitrary unit
CF	cystic fibrosis
CFTR	cystic fibrosis transmembrane conductance regulator
ECL	extracellular loop
ICL	intracellular loop
TMD	transmembrane domain
NBD	nucleotide binding domain
PKA	(cAMP-dependent) protein kinase A
RD	regulatory domain
Site 1	ATP-binding site 1
Site 2	ATP-binding site 2
PM	plasma membrane
ER	endoplasmic reticulum
PTC	premature termination codon
cAMP	cyclic adenosine monophosphate
ABC	ATP-binding cassette
MCC	mucociliary clearance
PAMP	pathogen-associated molecular pattern
DAMP	damage-associated molecular pattern
ROS	reactive oxygen species
MyD88	myeloid differentiation factor 88
AA.	arachidonic acid
$I_{sc}$	Short-circuit current

## **Chapter 1: Introduction**

## **1.1 Cystic fibrosis**

### **1.1.1 History of Cystic Fibrosis**

Cystic fibrosis (CF) was first recognized in 1938 [1]. The discovery of the cystic fibrosis transmembrane conductance regulator (CFTR) gene in 1989 was essential in advancing our understanding of disease pathogenesis and paving the way for treatments that target the underlying molecular defect. The understanding of the gene and its mutations, as well as the characterization of the CFTR protein and its function in the disease, have revolutionized the knowledge of ion transport pathophysiology in respiratory and digestive epithelial cells.

The earliest known cases of cystic fibrosis date to ancient Rome. However, significant advances in understanding the genetic basis and clinical manifestations of CF did not occur until the 20th century. Dr. Dorothy Andersen, a pathologist, made a revolutionary discovery in the 1930s when she identified cystic fibrosis as a distinct disorder [1]. Her innovative work set the groundwork for future CF research. Several other researchers made significant contributions to the understanding of CF during the 1940s and 1950s. Dr. Paul di Sant'Agnese discovered abnormal electrolyte levels in the perspiration of CF patients, which led to the development of the sweat test as a diagnostic tool for CF. Dr. Harry Shwachman elucidated the link between pancreatic insufficiency and cystic fibrosis [2].

The discovery of the genetic basis of cystic fibrosis (CF) in the late 1980s and early 1990s represented a significant changing point in CF research. In 1989, a team of scientists led by Dr. Francis Collins and Dr. Lap-Chee Tsui discovered the CF gene on chromosome 7, which encodes the cystic fibrosis transmembrane conductance regulator (CFTR) protein [3]. Mutations in this gene result in a defective CFTR protein, which is responsible for the CF symptoms. This breakthrough enabled further investigation into the molecular mechanisms underlying CF and eased the way for targeted therapies. Current research is leading to the development of new treatments such as CFTR modulator drugs that directly target the underlying defect in CF. While

there is still no cure for CF, significant advancement has been made in improving the quality of life for CF patients, thanks to the development of these therapies.

### **1.1.2 Cystic fibrosis clinical phenotype**

Cystic fibrosis (CF) is a lethal, autosomal recessive disease affecting over 4300 Canadians or roughly 1 in 3,600 live births. It is caused by mutations in the cystic fibrosis transmembrane conductance regulatory (or CFTR) gene. More than 2000 mutations have been identified in the CFTR gene [4-6]. Of the >800 mutants that have been analyzed in detail, >80% are disease-causing [4]. CF results in significantly reduced life expectancy. CFTR protein helps to maintain the epithelial surface hydration by mediating bicarbonate and chloride transport across the plasma membrane. Mutation in CFTR and loss of its function lead to disruption in the luminal  $\text{Cl}^-$  and  $\text{HCO}_3^-$  secretion [7]. CF as a multi-organ disease is responsible for pathologies, including the chronic deterioration of lung function brought on by recurrent respiratory infections and opportunistic microbial pathogen colonization of the airways, which results in dehydrated mucus and airflow obstruction of the lungs (Figure 1.1).

Additionally, loss-of-function of CFTR affects the reproductive and digestive systems. Due to decreased pancreatic enzyme output, people with CF may experience gastrointestinal symptoms linked to malabsorption of dietary nutrients, notably lipids. Some men with CFTR mutations may experience bilateral vas deferens absence in the reproductive system. The vas deferens have typically degenerated before birth due to blockage with thick mucus, even if these affected people are typically fertile (i.e., they do produce viable sperm) [8]. As a result, they would need assisted reproductive technologies to conceive.

### **1.1.3 Lung pathophysiology of CF**

When CFTR protein function is lost, mucus dehydration and hyperviscosity create a blockage of the airways [9]. This is followed by reduced mucociliary clearance (MCC) due to dysregulated  $\text{Cl}^-$ ,  $\text{HCO}_3^-$  and  $\text{Na}^+$  transport [9, 10]. This very sticky and thick mucus facilitates chronic infection and inflammation. Although persistent bacterial infection has long been known

to be the primary cause of airway inflammation in people with CF, the data indicates that inflammation in CF patients' lungs occurs before any infection, which supports the critical function of the CFTR protein. Studies in CF ferrets, CF newborns, and young children have demonstrated the presence of mucus obstruction and neutrophilic inflammation even in the absence of bacterial infection, suggesting that mucus obstruction in CF may result in sterile airway inflammation [9, 11, 12]. According to Balázs et al., thick and sticky mucus-induced hypoxia epithelial cell death may cause the production of IL-1 in CF airways [12, 13]. Chemokines like IL-8, which attracts neutrophils to the airways, are produced when this IL-1 signalling pathway is activated.

Following bacterial infection, both pathogen-associated molecular patterns (PAMPs) and damage-associated molecular patterns (DAMPs) activate immune cells including neutrophils, macrophages, and dendritic cells [9]. These events further facilitate the inflammatory response by inducing the synthesis and secretion of cytokines and chemokines (e.g., IL-1, IL-6, IL-8, and TNF- $\alpha$ ), as well as leukotrienes and prostaglandins from arachidonic acid (AA) metabolism. Neutrophils are the main immune cell type involved in this inflammatory process in CF. Neutrophils are crucial for antibacterial host defence, but they also create reactive oxygen species (ROS) and proteases, which can harm the lungs and cause a vicious cycle of inflammation [9]. The cytokine IL-17 is released by T cells during an adaptive immune response, controlling neutrophil recruitment and supplying more Th17 cells to the inflammatory response [14]. Additionally, individuals with CF have an overactive transcription factor called NF- $\kappa$ B, which results in the release of pro-inflammatory cytokines like IL-8 and the recruitment of neutrophils. By stimulating toll-like receptor (TLR) signalling and the myeloid differentiation factor 88 (MyD88), bacterial PAMPs induce NF- $\kappa$ B activation [9, 15]. Although there is a robust neutrophilic response, cystic fibrosis (CF) is distinguished by an increased susceptibility to lung infections and impaired bacterial clearance due to the dysfunctional CFTR protein [9]. Undoubtedly, CF leads to the impairment of two important airway defences, mucociliary clearance (MCC) and the innate immune system. This impairment is primarily caused by the dysregulated production of

bicarbonate ions ( $\text{HCO}_3^-$ ) [9]. These findings back up the recommendation to implement early preventative strategies in CF. The lack of CFTR-dependent anion transport/liquid secretion, which is likely responsible for the aberrant development of cartilaginous airways, can be utilized to account for the early limitation of airflow and the trapping of air in the CF [16-18]. The manifestation of lung injury in individuals with CF is evident during early childhood [19].

## **1.2 The CFTR structure**

CFTR is a member of the ATP-binding cassette (ABC) transporter family and functions as an anion channel [3]. The CFTR protein is composed of 1,480 amino acids in a single polypeptide chain that forms five functional regions, called domains (Figure 1.3A). It possesses two transmembrane domains (TMD1 and TMD2) as the basis of an anion conduction pathway, two cytoplasmic nucleotide-binding domains (NBD1 and NBD2) that bind and hydrolyze ATP [4], and an intrinsic disorder regulatory (R) domain. The R domain phosphorylation by the cAMP-dependent protein kinase (PKA) catalytic subunit represents the first step in CFTR channel opening (Figure 1.3A). Different conformations of CFTR's high-resolution three-dimensional (3D) structure have been determined by structural biology investigations (Figure 1.3B) [20].

## **1.3 Classifications of CFTR mutations**

According to the cellular phenotype, six classes of CFTR mutations are distinguished (Figure 1.4A) [21]. Class I mutations lead to no protein synthesis or translation of truncated forms. Class II mutations lead to a misfolded protein that fails to achieve its native conformation in the endoplasmic reticulum (ER). The conformationally defective channel is recognized by the ER quality control mechanism and, predominantly targeted for ubiquitin-dependent degradation by the proteasomes [22, 23]. Class III mutations lead to the channel gating defect due to impaired response to agonists and are characterized by a reduced open probability, although the protein can be present at the PM. Class IV mutations cause the channel conductance defect, impeding the ion permeation across the channel pore. Class V mutations lead to a reduction in protein abundance due to reduced synthesis or inefficient protein maturation by introducing promoter or

splicing abnormalities. Lastly, class VI mutations lead to reduced protein stability in post-ER compartments and/or at the PM. Figure 1.4B shows a recent classification of CFTR mutations recognizing the combinatorial defects in CFTR imposed by the mutations. The Venn diagram indicates all possible combinations of cellular defects (I-VI) with the most prevalent mutations' examples [21]. In the following section, I provide a short description of CFTR mutations that are utilized in my experiments.

$\Delta$ F508-CFTR: Even though cystic fibrosis is caused by most of the >2000 known mutations, ~90% of patients have at least one copy of the CFTR-F508del gene [6, 24]. A phenylalanine (F) residue is lost at position 508 of the CFTR protein as a result of the  $\Delta$ F508 (F508del) mutation. This mutation disrupts the normal folding and processing of the CFTR protein. The  $\Delta$ F508 mutant displays a severe trafficking defect resulting in intracellular retention and premature degradation of the channel [22]. The misfolded  $\Delta$ F508-CFTR protein is recognized by the cellular quality control systems, leading to its degradation in the ER and a decrease in the overall level of CFTR protein [25]. In addition, the few channels that reach the plasma membrane are unstable and dysfunctional. Therapeutic strategies for  $\Delta$ F508-CFTR aim to address the underlying folding and trafficking defects of the mutant protein. These include the application of CFTR correctors, which can improve the mutant CFTR protein's folding and maturation, and CFTR potentiators, which enhance the open probability of the mutant channels at the cell surface. Ongoing research efforts are focused on developing new therapies, such as modulators that can target both the folding and gating defects of  $\Delta$ F508-CFTR, as well as gene editing techniques that can correct the CFTR gene mutation itself.

G551D-CFTR: The amino acid glycine (G) is changed to aspartic acid (D) at position 551 of the CFTR protein because of this mutation. This mutation is located at the NBD1, and it disrupts the composite ATP-binding site 2, accounting for the compromised dimerization of the NBD1/NBD2 and the associated channel opening [26, 27]. Around 4 to 5% of individuals diagnosed with cystic fibrosis possess the G551D mutation on at least one allele [28, 29]. To treat

the G551D-induced functional defect, targeted treatments have been created. One such treatment modality is the CFTR potentiator Ivacaftor (VX-770), which improves the channel open probability.

N1303K-CFTR: At position 1303 of the CFTR protein, the amino acid asparagine (N) has been changed to lysine (K) in this common mutation with an incidence of 1.5% of all CF chromosomes [30]. This mutation is located in the NBD2 at the equivalent position, but in the opposite half of the CFTR molecule as the ΔF508 mutation. The N1303K mutation causes CFTR protein misfolding and misprocessing to the PM (Class II mutation), as well as severe gating defects (Class III). The gating defect can be explained by the N1303K-induced global misfolding of CFTR, including the NBD2 [31], which impairs the channel gating by interfering with the NBD dimerization [32, 33]. The N1303K-CFTR open probability amounts to 7-25% of the phosphorylated WT-CFTR [34, 35] which could be considered as a maximal value.

W1282X-CFTR: W1282X is the second most common nonsense mutation that causes CF [4] and the fifth most prevalent mutation in the CFTR gene that causes CF. Premature termination codons (PTCs) in the CFTR gene are present in over 7% of individuals with CF [36]. This PTC is responsible for truncating almost 60% of the NBD2 [37]. The W1282X nonsense mutation, also known as c.3846G>A, results in a shortened transcript that is vulnerable to nonsense-mediated decay (NMD), as well as a truncated protein that is misfolded and has severe gating defect if it reaches the PM [38, 39]. To treat the underlying abnormalities cellular and molecular defects of 1282X-CFTR, methods including small molecule correctors and potentiators, NMD suppressors, read-through facilitators, gene therapy, or gene editing techniques are being investigated [37, 40, 41].

S549R- and S549N-CFTR: The missense mutations of S549R and S549N occur at the nucleotide position c.1647 as a result of thymidine (T) to guanine (G) and at c.1646 as a result of guanine (G) to alanine (A) transversions, respectively. This mutation at the amino acid residue of 549 causes a replacement of serine by an arginine (R) or asparagine (N) in the NBD1 of the CFTR

structure [42]. The serine, which is a highly conserved amino acid at this position, facilitates ATP binding and hydrolysis. As a consequence, the S549R and S549N mutations lead to a pronounced gating defect. In addition, the S549R mutation also leads to mild a class II phenotype, where the abnormal protein fails to progress through the biosynthetic pathway and degrades at the ER [42].

WT 15SA-CFTR: According to the canonical CFTR activation model, phosphorylation of serine residues, which is predominantly accomplished by PKA-dependent phosphorylation, is a prerequisite to facilitate the dislocation of the R-domain from wedging between the NBD1 and NBD2 [43]. This CFTR variant was generated by replacing 15 serine- residues with alanine (15SA) in the Riordan lab [44]. To mostly inactivate the channel in our construct 15 Ser residues, representing mostly canonical protein kinase A (PKA) phosphorylation sites, were changed to Ala residues to interrogate the significance of these consensus phosphorylation sites in CFTR activation process by potentiators [45].

#### **1.4 CFTR function (activation, mechanism, gating cycles)**

Expression and activity of CFTR are regulated at multiple levels, and understanding the impact of regulatory and signaling pathways could improve the efficacy of existing therapies and facilitate the development of novel approaches. Different mechanisms regulate the activity of CFTR, such as the R domain dislodging gradually and spontaneously, which is then followed by phosphorylation that is reliant on PKA [20]. This leads to the opening of the channel by the ATP-induced dimerization of the NBD (Figure 1.5) [20]. The primary cellular signal for the CFTR canonical activation mechanism is the PKA-dependent phosphorylation of the channel. This process is initiated by the cytosolic elevation of the cyclic adenosine monophosphate (cAMP) concentration that triggers the dissociation of the PKA regulatory subunit from the catalytic subunit. The activated catalytic subunit then phosphorylates the CFTR's R-domain. Mutant CFTR can be potentiated without the PKA-dependent phosphorylation [46], but increasing cAMP levels

near CFTR can still have an additive effect and increase the potentiation sensitivity of the CFTR [47].

The CFTR channel activation is initiated, predominantly by the PKA activation [48], a prerequisite for the protracted displacement of the RD wedging between NBD1-NBD2 and cytoplasmic loops before NBD dimerization can occur [38, 45, 49-51]. Two ATP molecules, sandwiched between the Walker A and B sequence of one of the NBD and the signature sequence of the other NBD [49], stabilize the NBD1-NBD2 dimer, causing the rearrangement of the cytosolic loops and propagated conformational changes in the MSDs. In principle, this leads to the TMDs transition to the outwardly open configuration by rigid body motion in ABC exporters [52] and the formation of chloride translocation pathways formed by transmembrane (TM) helices TM1, 6, 8 and 12 [53] in CFTR [54]. The tetra-helix bundle becomes stabilized by electrostatic interaction between the CL2 and CL4 and facilitates the CFTR-activated state formation [55, 56]. ATP hydrolysis at the composite site 2, consisting of the NBD2 Walker motifs, contributes to the pore closing (Figure 1.5) [57].

## **1.5 CFTR pharmacotherapy FDA-approved and investigational modulators**

### **1.5.1 CFTR potentiators**

As a CFTR potentiator, VX-770 (Ivacaftor, brand name Kalydeco; developed by Vertex Pharmaceuticals in collaboration with the CF foundation) enhances CFTR activity by raising the channel's open probability ( $P_o$ ) [58]. The potentiator VX-770 showed strong clinical efficacy in enhancing respiratory function, and it was initially licensed for individuals with G551D mutation. The fact that VX-770 potentiates the most prevalent G551D class III mutation implies that the drug's activity is unrelated to ATP hydrolysis or NBD dimerization [59, 60]. A 10% increase in predicted FEV1, a 55% decrease in the frequency of pulmonary exacerbations, and a decrease in sweat chloride concentration (to an average concentration below the diagnostic threshold of 60 mM) are all indications that VX-770 improved lung function in CF patients with the G551D mutation [61]. Additional FDA approval has been granted for several other class III (gating)

mutations (e.g., G1244E, G1349D, G178R, G551S, S1251N, S1255P, S549N, and S549R), as well as to the conductance class IV mutation R117H. Since the approval of VX-770, other potentiators with intriguing pharmacological qualities have started clinical trials, including QBW-251 (by Novartis) and GLPG1837 (by Galapagos NV) (Figure 1.8). The binding site of VX-770 on the CFTR has been identified by cryo-EM as illustrated in Figure 1.10.

Several groups, including ours, have shown that the VX-445 corrector has gating potentiator activity and has an additive effect with VX-770 in potentiating Class III and IV CFTR mutations (represented by G551D and R117H mutations, respectively) using primary human airway epithelia and model cells recombinantly expressing CFTR, suggesting that these two drugs have different mechanisms of action in potentiating CFTR [62-64].

Figure 1.9 illustrates the results of our combinatorial profiling approach with cluster analysis of known potentiators to classify whether their mechanism of action is additive or not. This was accomplished by comparing the combined effects of pairwise potentiator combinations to the theoretical and de facto additive activation of mutant CFTRs at saturating concentration using cluster analysis. VX-770 exhibits neither additivity nor redundancy toward the ABBV-974 as class I potentiators. bDMC (bis-demethoxy-curcumin) and apigenin exhibit neither additivity nor redundancy, as class II potency. As a class III potentiator, VX-445 exhibits additivity or partial additivity with class I or class II potentiators. This is done on the CFBE41o- YFP by Veit et al. [63].

As the cluster analysis suggested three distinct classes of potentiators regarding their gating activation, it is plausible to assume that some of the therapy-resistant or poorly responsive mutants can be rescued by a triple combination of potentiators, a hypothesis that will be tested in my thesis.

### **1.5.2 CFTR correctors**

The therapeutic success of VX-770 encouraged the development of pharmacophores that can correct CFTR conformational defects. The F508del variant, the most prevalent CF-causing

mutation, attracted a lot of interest.  $\Delta$ F508-CFTR processing defect and functional expression at the PM can be recovered to 15% of WT-CFTR by exposure to low temperature and chemical chaperones, as well as the introduction of second-site suppressor mutations into the NBD1 [31, 65-68]. High Throughput Screening (HTS) of small drug-like compound libraries in combination with medicinal chemistry led to the development of CFTR correctors or pharmacological chaperones that can facilitate the folding and processing of class II CFTR mutants at the ER and correction of the loss-of-function PM defect of  $\Delta$ F508 and other folding mutations [69].

The first clinical trials reporting the efficacy of the VX-809/VX-770 combination drug, sold under the name Orkambi, were reported in 2015 [70, 71]. The approval was expanded to include patients as young as 2 years old by 2018. The efficacy of Orkambi for the correction of F508del CFTR is limited, in part due to the destabilizing action of VX-770 long-term exposure [72]. Similarly, destabilization of a subset of class II mutations, including P67L, E92K, R170G, S341P, D614G, and S1235R, upon long-term VX-770 exposure has been reported [72-75]. In contrast, G551D-CFTR and other gating mutants are not affected by this VX-770 adverse side effect, indicating that the VX-770 destabilizing effect is mutation-dependent.

Other correctors have been found, such as VX-661 (Tezacaftor; Vertex Pharmaceuticals), which is structurally related to VX-809 but has better pharmacokinetic and safety characteristics. The VX-661/VX-770 combination (marketed under the brand Symdeko) was given FDA approval in 2018 for the treatment of F508del-homozygous individuals and those with at least one residual function mutation from a predetermined list. Figure 1.11 illustrates the increase in CFTR activity that arises from a combination of correctors and potentiators. They discovered through short-circuit current recordings that the dual-acting chemical (bottom trace) boosts both the overall current and the percentage of the current that is triggered by cAMP alone, thus reducing the need for a potentiator [76].

The third-generation corrector VX-445, which was recently developed by Vertex Pharmaceuticals, functions additively to VX-809 or VX-661 by binding to the MSD1/2 interface

[74, 77, 78]. Other correctors developed by Galapagos and Proteostasis Therapeutics, either as monotherapies or as components of combination therapies, are now being examined in the clinic. Recent research from our group has demonstrated the effectiveness of a triple corrector combination for the missense mutations  $\Delta F508$ -CFTR and rare CFTR2 mutants, finding three new correctors (6258, 4172, and 3151) [79]. Type I correctors (such as VX-809, C3, and 6258) target the NBD1-TMD1/2 interface to allow cooperative domain assembly. Type II correctors (such as C4 and 3151) affect NBD2 and the points at which it connects to other CFTR domains. Compounds that specifically target the NBD1 (like 4172) are classified as Type III correctors. The chemical structures of some correctors are shown in Figure 1.7, and the binding sites of VX-661 and VX-445 in a CFTR cryoEM structure on Figure 1.10.

The FDA approval of medications that treat the underlying CFTR protein deficiency has had a substantial impact on the treatment approaches for CF (Figure 1.6). With the discovery of small molecule drugs that assist the (partial) repair of mutant CFTR trafficking and channel function, significant advancements have been made. A few years after the first medicine, VX-770, that potentiated the CFTR channel activity, the majority of CF patients were able to get an efficient modulator therapy. Trikafta, a triple combination drug, was initially approved for patients who had at least one copy of the F508del CFTR allele. More recently, Trikafta was approved for an additional > 150 rare mutations. Despite this, the drug does not improve mutant CFTR function to the WT level nor completely alleviate CF symptoms. In addition, many rare mutations are only marginally responsive or not responsive to modulator drugs that are currently on the market. Figure 1.8 summarizes some of the mutations that have not been approved for treatment with modulators.

### **1.5.3 The cAMP-elevating agent and inhibitors**

The cAMP-dependent enzyme protein kinase A (PKA) phosphorylates CFTR. Following an increase in intracellular cAMP, PKA is activated and can phosphorylate CFTR, increasing the

probability of an open channel. The cAMP-efflux transporters, phosphodiesterases (PDE), and  $\beta$ 2 adrenergic receptors are only a few of the systems that regulate cAMP.

CFTR<sub>inh</sub>-172 is a potent and fairly selective inhibitor of CFTR. It prevents CFTR's chloride ion permeation. CFTR<sub>inh</sub>-172 is frequently used by researchers in lab settings to investigate CFTR function or to confirm CFTR involvement in particular physiological processes [80].

### **1.6 CFTR gating mutations, mechanism, and mechanism of rescue theories**

Genetic modifications called CFTR gating mutations impact how the CFTR chloride ion channel opens and closes (gates). Gating mutations cause the channel to improperly regulate ion flow, which causes the mucus in the airways to thicken and affects the fluid balance in numerous organs. One of the numerous genetic changes linked to CFTR gating mutations. A gated chloride channel is created by the CFTR protein. It responds to a variety of cellular signals, including cAMP, which is involved in the control of ion transport, by opening and closing. The normal operation of this channel is interfered with by CFTR gating mutations that change the structure or function of the protein. Ion transport may become dysfunctional as a result of the channel remaining closed when it should be open or remaining open when it should be closed. There are two broad categories in which to place gating mutations. First off, there are gating mutations that have a decreased chance of the CFTR channel being in the open state, which results in less chloride ion transport. Ion flow across the cell membrane is hampered by this channel's insufficient opening. Second, CFTR channel gating mutations with enhanced open probabilities, where the channel is more likely to remain in the open state even when the proper cellular signals are absent. This leads to aberrant chloride ion transport and can cause a significant amount of ion loss. The goal of rescue theories is to reverse the detrimental CFTR gating alterations and restore normal channel operation. To cope with these mutations, several tactics have been created, including potentiators, correctors, and a combination of them. Particularly for those with gating mutations, rescue theories and the development of CFTR modulator medications have revolutionized the management of cystic fibrosis. These treatments have improved lung function,

decreased symptoms, and improved quality of life for many people with CF by focusing on the underlying CFTR abnormalities.

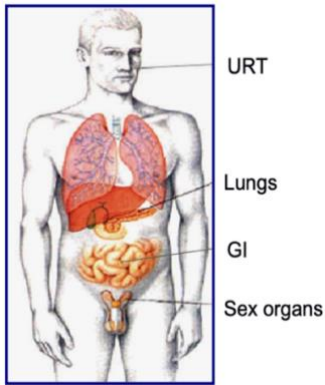


**Figure 1.1. Organs affected by cystic fibrosis (CF).** Chronic Sinusitis and nasal polyps are upper respiratory tract (URT) CF-related diseases. Dehydrated mucus, impaired mucus clearance, and airflow obstruction are lung CF-related diseases. Pancreatic insufficiency (malnutrition, diabetes), biliary cirrhosis and portal hypertension are examples of gastrointestinal (GI) tract CF diseases. Congenital bilateral absence of the vas deferens is one of the most common CF-related sex organ diseases [7-9].

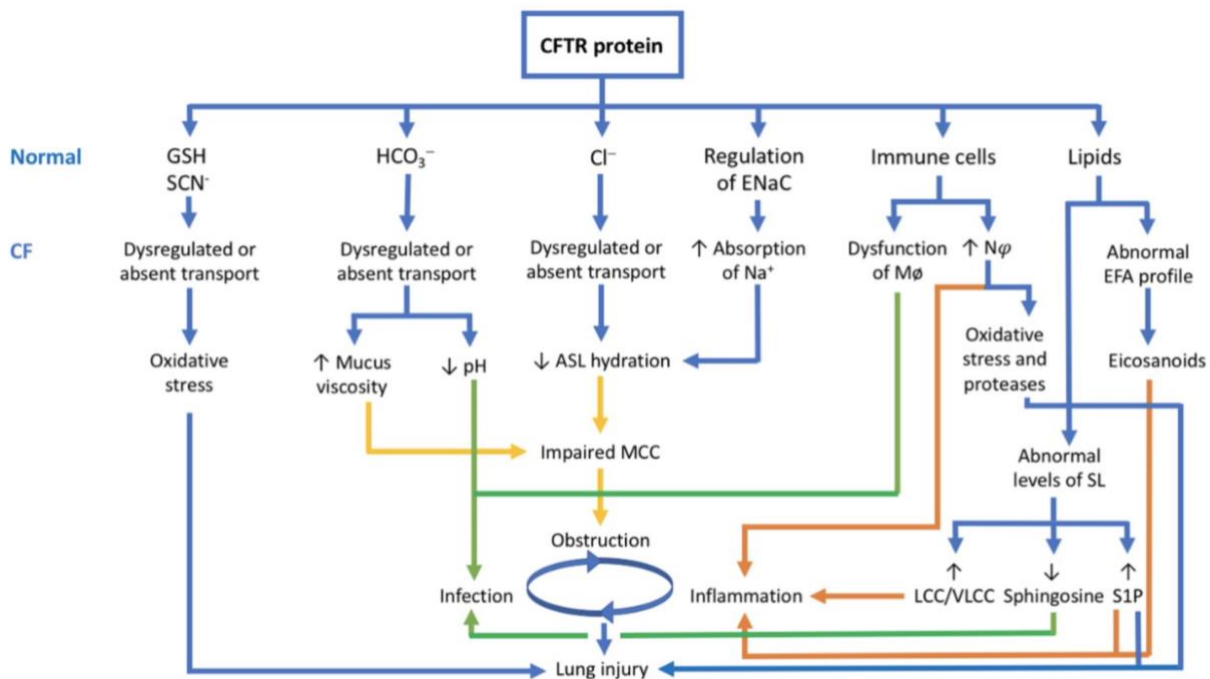


**Figure 1.2. Relationship between CFTR protein and lung pathophysiology of CF.** A chloride channel is not all that the CFTR protein is. Additionally, it is involved in the transfer of HCO<sub>3</sub>, GSH, and SCN<sup>-</sup>, the control of ENaC, immune cells, and lipid metabolism. Bronchial obstruction (shown in yellow), inflammation (shown in orange), and infection (shown in green) are caused by the loss of functioning CFTR in CF, which culminates in lung damage. Abbreviations: Cl<sup>-</sup> = chloride; HCO<sub>3</sub><sup>-</sup> = bicarbonate; GSH = glutathione; SCN<sup>-</sup> = thiocyanate; Na<sup>+</sup> = sodium; ENaC = epithelial sodium channel; ASL = airway surface liquid; Mφ = macrophages; Nφ = neutrophils; SL = sphingolipids; S1P = sphingosine-1-phosphate; LCC/VLCC = long-chain ceramides/very long-chain ceramides. Reproduced from [9].

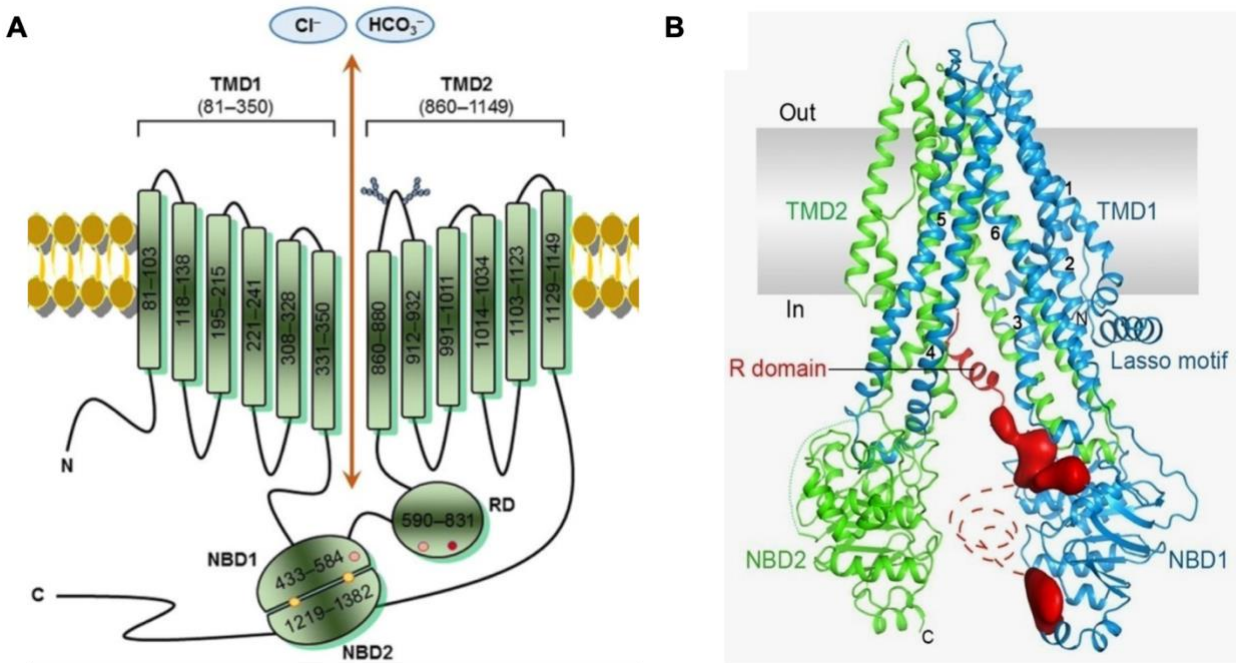


**Figure 1.3. Topology and CryoEm structure of the CFTR. A)** Topology of the CFTR in the plasma membrane. MSD1 and MSD2, shown in green, are the two membrane spanning domains composed of six transmembrane (TM) domains each. The four intracellular loops, ICL1 to ICL4, are indicated. The nucleotide binding domains, NBD1 and NBD2, are represented at the bottom, and the regulatory domain, RD is depicted in a circle. Reproduced from [81] with permission from © 2016 Lopes-Pacheco. **B)** The CryoEM structure of the CFTR channel. The CFTR protein contains a single chain of amino acids, consisting of two TMDs and two NBDs and a regulatory (R) domain which is wedged between the two NBDs. Reproduced from [78].

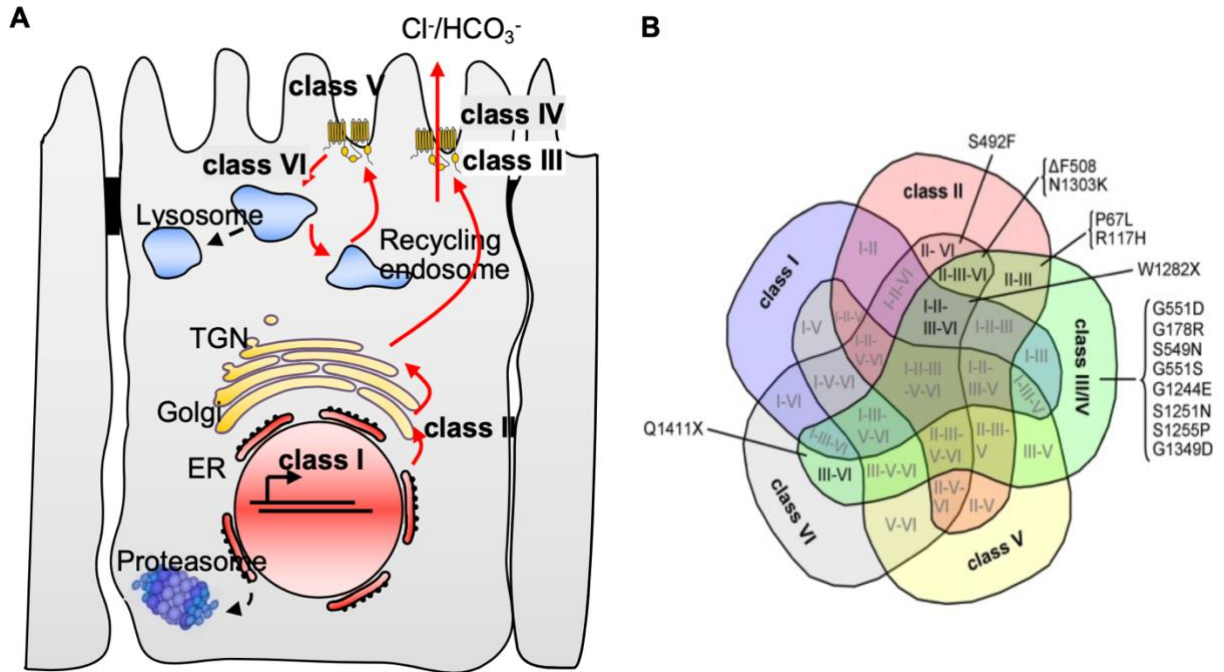


**Figure 1.4. Classification of CFTR mutations depicting fundamental molecular defects.**

**A)** Schematic diagram illustrating the six classes of CFTR mutations based on their cellular phenotype: class I: defects in protein synthesis; class II: maturation defect; class III: gating defects; class IV: conductance defects; class V: a reduction in the amount of functional CFTR; and class VI: a reduction in peripheral stability ER, endoplasmic reticulum; TGN, *trans*-Golgi network. Reproduced from [21] with permission from ascb MBoC under an Attribution-Noncommercial-Share Alike 3.0 Unported Creative Commons License. **B)** Refined classification of CFTR mutations that acknowledges the combinatorial deficiencies in CFTR induced by the mutations. The Venn diagram illustrates many examples of cellular defects (I–VI) in all possible combinations. Reproduced from [21] with permission from ascb MBoC under an Attribution-Noncommercial-Share Alike 3.0 Unported Creative Commons License.

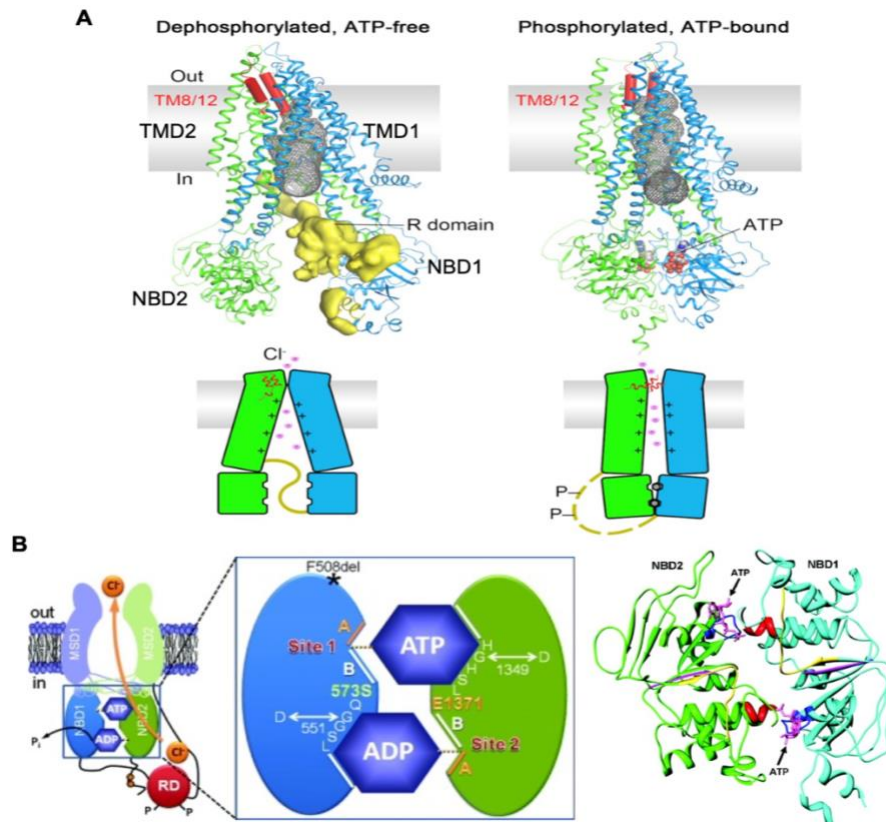


**Figure 1.5. Activation of CFTR channel.** **A)** The cryoEM structures of the hypothesized closed (left) and open (right) conformations of the CFTR channel. The closed conformation of CFTR is represented by the structure of unphosphorylated, ATP-free CFTR (PDB: 5UAK; [78]), whereas the open conformation is represented by the structure of phosphorylated, ATP-bound CFTR (PDB: 6MSM; [51]). Notably, the overall design of the ATP-bound CFTR structure should closely resemble an open conformation even if the pore is too small to allow the passage of a dehydrated chloride [51]. The grey rectangles stand in for the lipid bilayer. In and out denote the intra- and extracellular sides of the membrane, respectively [82]. **B)** The arrangement of the CFTR's ATP-binding sites in an open CFTR Cl channel, the simplified model depicts the molecular structure of ATP-binding sites 1 and 2. The Walker A and B motifs (designated A and B, respectively) of one NBD and the LSGGQ motifs of the other NBD combine to form each ATP binding site. Site 1 has a non-canonical LSGGQ motif (LSHGH), whereas site 2 has a canonical LSGGQ motif. A catalytic base (E1371) is also present at site 2 at the distal end of the Walker B motif, whereas this residue is missing from site 1 (S573). The G551D (site 2), G1349D (site 1), and F508del (surface of NBD1 opposing ICL4) CF mutations' locations are depicted. Abbreviations: P, phosphorylation of the RD; P<sub>i</sub>, inorganic phosphate; RD, regulatory domain. Reproduced from [48].

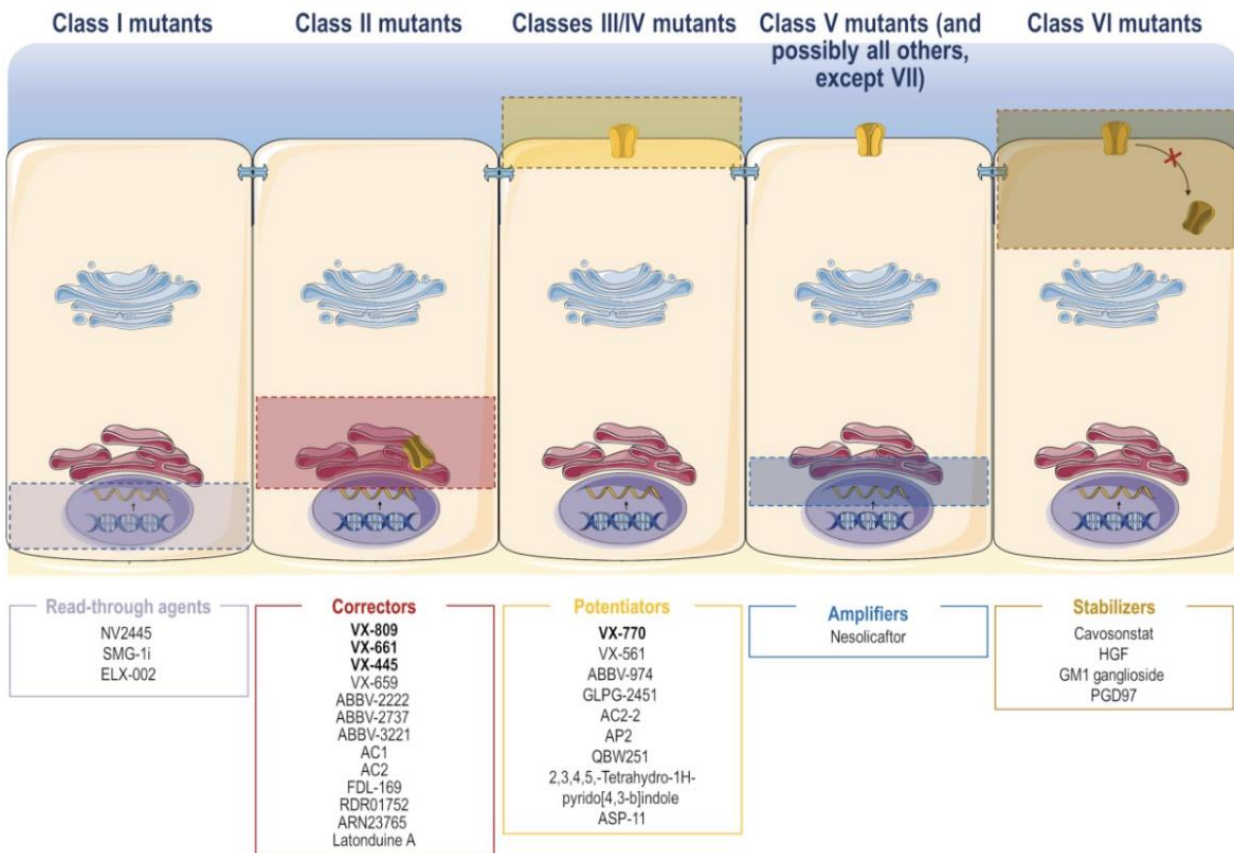


**Figure 1.6. CFTR pharmacotherapy FDA-approved and investigational modulator.** The CFTR modulators include correctors, potentiators, amplifiers, stabilizers, and read-through agents. Schematic diagram illustrating the six classes of CFTR mutations based on their cellular phenotype and their corresponding available therapies. Reproduced from [81].

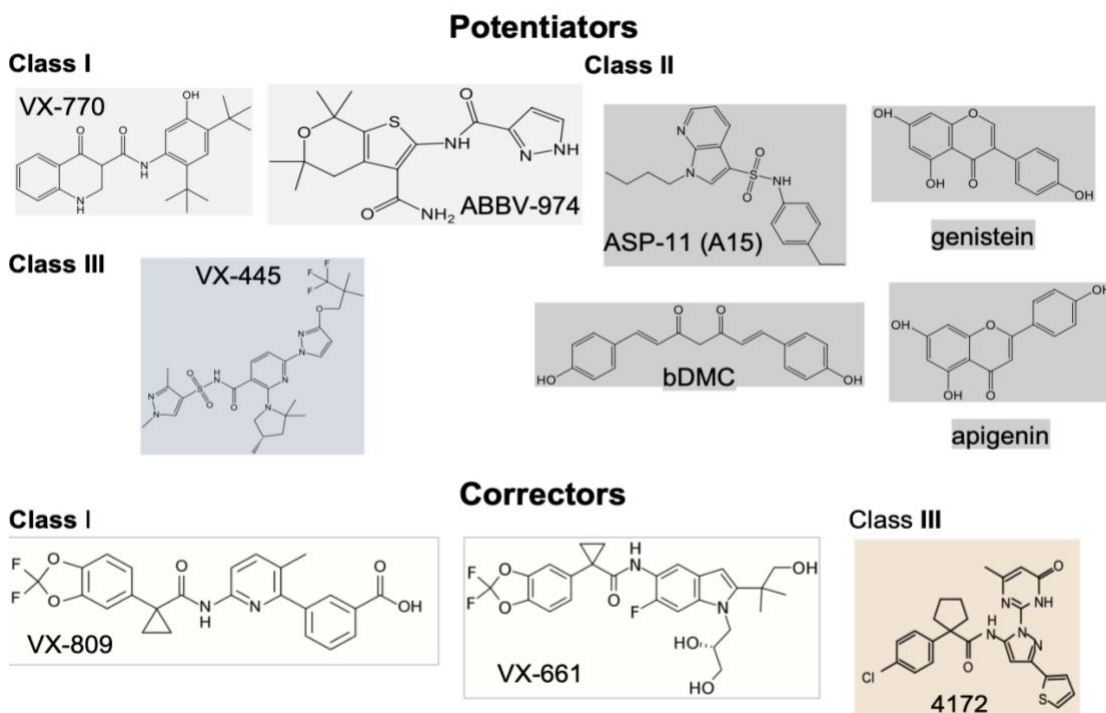


**Figure 1.7. Chemical structures of CFTR modulators are commonly used.** Chemical structures of the correctors and potentiators that are mainly used in CFTR research. Folding correctors mechanism of action indicated, class I, supports the formation of NBD1-TMD1 and NBD1-TMD2 interfaces; class II, restores NBD2 stability and its interfaces with other CFTR domains; and class III, facilitates NBD1 folding ([79, 83], permission from Nature Medicine and Journal of Cystic Fibrosis, respectively).

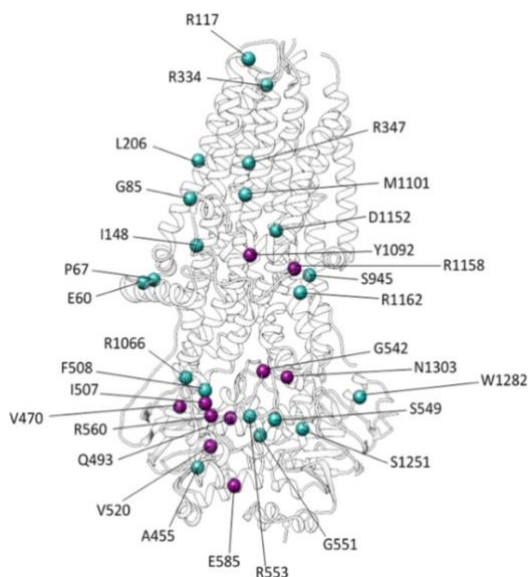


**Figure 1.8. Location of the most prevalent single-point CFTR variants mapped onto the CFTR structure.** The structure of the phosphorylated and ATP-bound human CFTR (PBD ID: 6MSM) is shown in light gray, with the positions of the 30 most common single amino acid variants depicted as spheres. CFTR variants approved for treatment with the triple combination therapy elexacaftor-tezacaftor-ivacaftor (Trikafta, Kaftrio) are shown in cyan, and variants not yet approved for modulator treatment in purple. Reproduced from [84] with permission from Springer Nature journal.

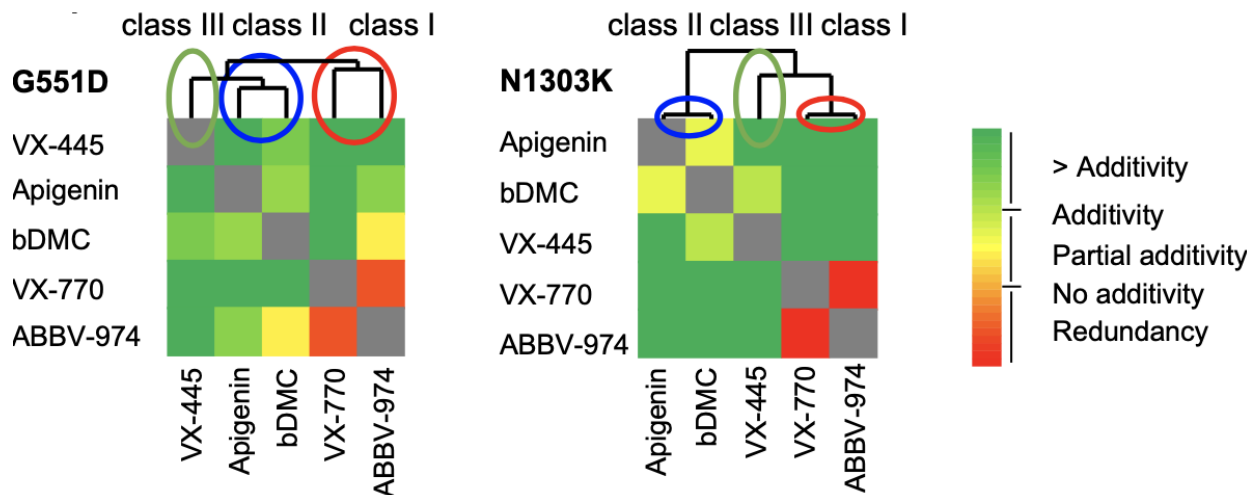


**Figure 1.9. Combinatorial profiling to classify potentiator mechanisms of action based on their additive activation of CFTR gating mutants.** Combinatorial profiling of compound pair effect on G551D-, and N1303K-CFTR activity in comparison to their theoretical additivities. VX-770 shows no additivity or redundancy to ABBV-974, a class I potentiator. VX-770 and ABBV-974 show a class I potentiation. Apigenin and bDMC show no additivity or redundancy, a class II potentiation. VX-445 shows additivity or partially additivity to other potentiators, as a class III potentiator. This profiling is performed on CFBE41o- co-expressing the indicated mutant and the halide-sensitive YFP (n=3 independent experiments, n=4 technical replicates). Reproduced from [63] with permission from Elsevier Journal.

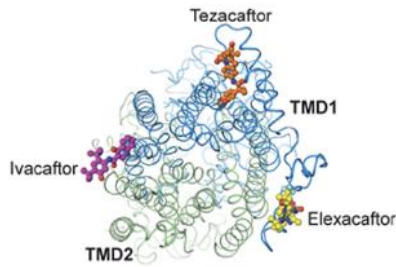


**Figure 1.10. Binding sites of VX-770 (purple), VX-661 (orange), and VX-445 (yellow) in the CFTR structure (CryoEM, EMD-28161, [85]).**

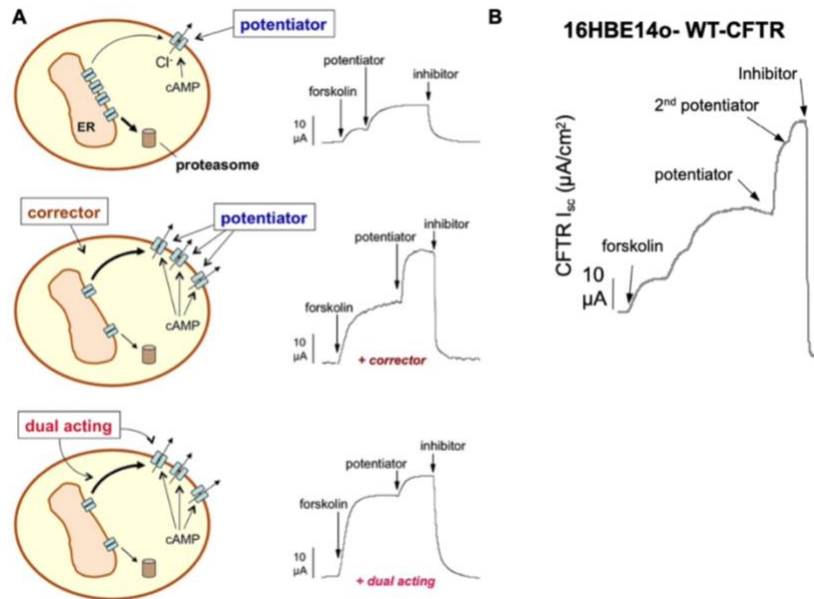


**Figure 1.11. Pharmacological rescue of folding and gating mutations. A)** As an example, long-term administration of a corrector, a tiny chemical that releases F508-CFTR from the endoplasmic reticulum (ER) and/or lengthens the protein's half-life in the plasma membrane, may increase the activity of F508-CFTR in the PM. By using a variety of technologies, including electrophysiological methods to directly measure Cl<sup>-</sup> currents (such as the short-circuit current recordings shown in the Figure), it is possible to assess a corrector's impact at the functional level. Forskolin is used to initially stimulate CFTR activity. A potentiator, a substance that fixes the intrinsic channel gating defect brought on by F508, is then used to further increase CFTR activity. Finally, the total Cl<sup>-</sup> current reliant on CFTR is then measured using an inhibitor of CFTR. Because there are more CFTR channels in the PM after incubation with a corrector, the total current (middle trace) is enhanced. A dual-acting substance (bottom trace) reduces the need for a potentiator by increasing both the total current and the percentage of the current that is triggered by cAMP alone. Reproduced from [76] with permission from Front Pharmacol under the Creative Commons Attribution License. **B)** An example of WT-CFTR I<sub>sc</sub> activation by forskolin and dual potentiators in 16HBE14o- cells.

## **Chapter 2: Rationale and Hypothesis**

A significant number of rare CF mutations have limited or no susceptibility to the approved CFTR-modulator treatment. Hence, it is necessary to evaluate if the channel function of these CFTR variants may be restored by preclinical compounds that enhance their activity or rectify their defects. Furthermore, a comprehensive knowledge of the mechanism of action of CFTR modulators may guide the selection of improved modulator combinations and provide a rational basis for the use of modulator treatment of rare mutations. Our laboratory has identified a novel CFTR corrector molecule, known as 4172 [79] that also has modest gating potentiator action. Preliminary data also suggested that 4172 displays a different mechanism of action (MOA) as compared to that of VX-770 (class I) and VX-445 (class III). Specifically, 4172 acts as a class II potentiator, similar to other known class II potentiators (e.g., apigenin, bDMC; some have low efficacy and limited absorption into the bloodstream), which form a distinct class of compounds based on their functional additivity to the class I potentiator. Our hypothesis was that by studying the structure-activity relationship (SAR) of a panel of 4172 analogs, we may identify new lead compounds that can improve the functional rescue of a subset of CFTR gating defect as a co-potentiator. Furthermore, we also hypothesized that the 4172 analogs similar to the known potentiators act by binding to CFTR transmembrane domains and may bypass the canonical activation mechanism of the channel.

## **Chapter 3: Methods and Materials**

### **3.1 CFTR modulators and antibodies**

CFTR modulators VX-770 and VX-661 were purchased from Selleckchem. VX-445 and ABBV-2222 were synthesized as described in Veit G., et al. [86]. 4172 was acquired from Life Chemicals and its analogs from Dr. G. Marzaro's group (University of Padua). CFTR<sub>Inh</sub>-172 was purchased from Tocris Bioscience. Forskolin is a adenylate cyclase activator. Isobutylmethylxanthine (IBMX) is a general phosphodiesterase (PDE) inhibitor [87]. Both forskolin and IBMX were purchased from MedChemExpress.

The following antibodies were used: monoclonal mouse anti-CFTR (L12B4; Chemokine, East Orange, NJ), monoclonal mouse anti-HA (MMS101R; Covance, Berkeley, CA), and monoclonal mouse anti-Na<sup>+</sup>/K<sup>+</sup>-ATPase (H3; Santa Cruz Biotechnology).

### **3.2 Cell lines and tissue culture**

#### **3.2.1 Human bronchial epithelia (CFBE41o-) and inducible variants**

The Human bronchial epithelia CFBE41o-cells (a gift from D. Gruenert, UCSF, San Francisco, California, USA) were engineered to express inducible CFTR variants with a 3HA-tag in the fourth extracellular loop as described [88-90]. By using overlapping PCR mutagenesis to introduce nucleotide changes, new CFTR variants were created [83]. Sanger sequencing was used to validate the PCR-amplified constructs at the McGill Genome Center.

The Lenti-X TetON Advanced Inducible Expression System (Clontech, Mountain View, CA) was used following the manufacturer's instructions to create lentiviral particles to transduce the CFBE41o- cell line and generate inducible CFTR (iCFTR) expressing cell lines. The plasmid containing halide-sensitive yellow fluorescence protein (YFP-H148Q/I152L/F47L) cDNA was cloned into the constitutive lentiviral vector pLVX-IRES-Hyg and used to co-transduce the iCFTR expressing CFBE41o- cells as described [89, 91].

The CFBE41o- cells were grown at 37°C in fetal bovine serum (FBS; Invitrogen), 10%, 2 mM L-glutamine (Sigma), and 10 mM 4-(2-hydroxyethyl)-1-piperazineethanesulfonic acid (HEPES)-supplemented Minimum Essential Medium MEM (Invitrogen). For growth, the cells were

cultured in plastic flasks coated with an extracellular matrix (ECM mix) made up of 250 µg/ml bovine serum albumin (Sigma-Aldrich) diluted in LHC basal medium (Invitrogen), 30 µg/ml PureCol collagen preparation (Advanced BioMatrix, San Diego, CA), and 10 µg/ml human fibronectin (EMD, San Diego, CA). For stable cell line selection of the infected CFBE41o- iCFTR-3xHA/YFP, 200µg/ml G418 (Invivogen #ant-gn-5), 3µg/ml puromycin (Invivogen #ant-pr-5), and 200µg/ml hygromycin B were added to the media. Millipore Sigma's 500 ng/ml doxycycline was used to induce the expression of CFTR variations for three days or more. The freezing medium consisted of 25 ml medium, 20 ml FBS, and 5 ml DMSO per 50 ml.

Handling the cells and preparing for halide-sensitive YFP assay is described below. First, the cells were propagated by splitting at a 1:2 – 1:5 ratio every 2-4 days after rinsing with DPBS (Gibco #14190), and trypsinization with TE Gibco 15400 1:10 in DPBS. The medium was changed in cultured cells every 2 days.

Preparing the cells for experiments on 96-well plates was done as follows. On day 0, the cells were seeded onto 96-well plates at a density of 20,000 cells/well (10 cm dish yields ~ 2x10<sup>6</sup> cells, sufficient for ~ 100 wells), using 100µl cell suspension and incubating at 37°C for 12-24h, with no cell and non-induced cell or TetON-only cell wells as controls. Doxycycline (Sigma D-9891, solved in H<sub>2</sub>O, sterile filter) induction of CFTR expression was started on Day 1 at 500 ng/ml doxycycline concentration in medium (200 µl/well) incubating at 37°C for 48h. On day 3 fresh medium was added with doxycycline and incubated for an additional 48h at 37°C. On day 4 the medium was replaced again and incubated further for 24h with doxycycline and, if required, with the corrector VX-661 (3 µM) at 37°C. CFTR chloride transport activity was measured on day 5. Notably, doxycycline stock is prepared (1000x) 500µg/ml in H<sub>2</sub>O and stored in aliquots at -20°C, and is added every time fresh to the medium because it is unstable.

### **3.2.2 Human bronchial epithelia (16HBE14o-), gene-edited variants**

Parental 16HBE14o- were obtained from D. Gruenert (University of California, San Francisco). The gene-edited 16HBE14o- (16HBEge) containing the G551D or N1303K mutation

in the CFTR gene, was provided by the CFFT and has been described before [58, 88, 89, 92]. Cells were cultured in the same medium as the CFBE41o- cells as described above without selection.

### **3.2.3 Human nasal epithelial (HNE) primary cells**

HNE isolation from both healthy human subjects and individuals with CF was conducted under the approved protocol and consent form from the McGill MUHC Research Ethics Board (14-234-BMB). We strictly adhered to all pertinent ethical regulations. The process of tissue collection and isolation of HNE cells was carried out as described by Muller L., et al. [93]. Subsequently, HNE cells were conditionally reprogrammed and differentiated on Snapwell filter supports for running short circuit current measurements ( $I_{sc}$ ) in the Ussing chamber setup [94, 95].

### **3.3 Immunoblotting and protein analysis**

To prepare CFTR-3HA-expressing CFBE cell lysate for immunoblotting, RIPA buffer (150 mM NaCl, 20 mM Tris-HCl, 1% Triton X-100, 0.1% SDS, and 0.5% sodium deoxycholate) was used, including protease inhibitors (10 mg/ml leupeptin, 10 mg/ml pepstatin). Cell lysates were centrifuged for 15 minutes at 14,000 rpm (4°C) to remove insoluble debris. Protein concentration was measured using the BCA assay and the lysates were denatured using 2X Laemmli sample buffer (LSB) by dilution with 10X LSB. Specific protein amounts and Precision Plus Protein™ Dual Color Standards were separated on a 7% SDS-PAGE. The following antibodies were used for probing the nitrocellulose membrane with enhanced chemiluminescence (ECL) kit from Bio-Rad: anti-HA monoclonal antibody (1:1000, clone MMS101R, Covance) for CFTR-3HA and monoclonal mouse anti-Na<sup>+</sup>/K<sup>+</sup>-ATPase (1:1000, H3; Santa Cruz Biotechnology) as a loading control, followed by anti-mouse IgG conjugated to horseradish peroxidase (Jackson ImmunoResearch Lab INC). The ChemiDoc MP imaging system was used to acquire the images from nitrocellulose membranes, and quantitatively analyzed by the ImageJ (NIH) program. The immunoblots of all cell lines used in this project are shown in Figure S.1.

### 3.4 Functional assays to detect CFTR activity

#### 3.4.1 Short-circuit current ( $I_{sc}$ ) measurement

CFBE41o- cells were plated on ECM-coated 12-mm Snapwell filters (Corning, Figure 3.1A) at a density of  $\sim 100,000$  cells/cm<sup>2</sup>. The  $\sim 4$  days post-confluent polarized epithelia were mounted in Ussing chambers and submerged in Krebs-bicarbonate Ringer (KBR). Continually bubbled with 95% O<sub>2</sub> and 5% CO<sub>2</sub>, the solution contained 140 mM Na<sup>+</sup>, 120 mM Cl<sup>-</sup>, 5.2 mM K<sup>+</sup>, 25 mM HCO<sub>3</sub><sup>-</sup>, 2.4 mM HPO<sub>4</sub>, 0.4 mM H<sub>2</sub>PO<sub>4</sub>, 1.2 mM Ca<sup>2+</sup>, 1.2 mM Mg<sup>2+</sup>, and 5 mM glucose (Table 3.1). A schematic representation of an epithelial monolayer mounted in the Ussing chamber is shown in Figure 3.1B. NaCl was substituted with Na<sup>+</sup>-gluconate to impose a chloride gradient.

We applied 100  $\mu$ M amphotericin B to the basolateral domain to enable the isolation of apical membranes for CFBE41o- cells, allowing for the measurement of stimulated CFTR activity. In the case of 16HBE14o- cells, no permeabilization was performed. We utilized the Acquire and Analyze package from Physiologic Instruments in San Diego, CA, to record short circuit current ( $I_{sc}$ ) measurements. These measurements were conducted at 37°C under  $I_{sc}$  conditions and were expressed as current per square centimetre.

Unless specified otherwise, to ensure that the measured current represents CFTR activity, the transepithelial Na<sup>+</sup> transport through epithelial Na-channel (ENaC) was blocked by 100  $\mu$ M amiloride, an ENaC inhibitor. A schematic of the Ussing chamber setup and the impact and effective plasma membrane side of each compound is shown in Figure 3.1C. The transepithelial voltage was clamped at 0 mV after correcting for voltage and is reported as A/cm<sup>2</sup>, using the Analyze software program (Physiologic Instruments, San Diego, CA). Following the addition of forskolin (20  $\mu$ M) and the potentiators VX-770 (3  $\mu$ M), other potentiators were added as described in the Results. At the end of each experiment, CFTR was inhibited with CFTR<sub>inh</sub>-172 (20  $\mu$ M) to demonstrate the  $I_{sc}$  CFTR specificity. Potentiator dose responses were established using a range of 0.1, 0.3, 1, 3, 10, and 30  $\mu$ M of the indicated potentiators. In addition, sequential

Table 3.1. Krebs-bicarbonate solution for Ussing chamber.

	MW (g/mol)	Apical (mM)	Basolateral (mM)
NaCl	58.44	-	115
Na-D-gluconate	218.1	115	-
NaHCO <sub>3</sub>	84.01	19.8	19.8
KHCO <sub>3</sub>	100.12	5.2	5.2
Na <sub>2</sub> HPO <sub>4</sub>	141.96	2.4	2.4
CaCl <sub>2</sub> (2H <sub>2</sub> O)	147.02	1.2	1.2
MgCl <sub>2</sub> (6H <sub>2</sub> O)	203.3	1.2	1.2
Glucose	180.16	5	5
NaH <sub>2</sub> PO <sub>4</sub>	120	0.4	0.4

acute additions of forskolin (0.03, 0.1, 0.3, 1, 3, 10  $\mu\text{M}$ ), genistein (50  $\mu\text{M}$ ), or VX-770 (10  $\mu\text{M}$ ), followed by the inhibition of CFTR with CFTR<sub>inh</sub>-172 (20  $\mu\text{M}$ ) were used to quantify CFTR-dependent constitutive (or residual) and forskolin-activated currents (Figure 3.2).

### **3.4.2 CFTR activity measurements by the halide-sensitive yellow fluorescent protein (YFP) assay**

CFBE41o- cells, co-expressing the indicated CFTR variant and the halide-sensitive YFP were seeded in 96-well plates and cultured for 4-5 days as described in Methods before the fluorescence measurements. Cells were washed 4 times with DPBS with  $\text{Ca}^{2+}$  and  $\text{Mg}^{2+}$  with a plate washer, then treated with the indicated potentiator in a volume of 50  $\mu\text{l}$  per well, and incubated at room temperature for 5-10min. CFTR phosphorylation was stimulated by 20  $\mu\text{M}$  forskolin and 500  $\mu\text{M}$  IBMX upon addition by injection into the well by the plate reader, while the basal YFP fluorescence was continuously measured using the FLUOstar Omega (BMG Labtech) multidetection microplate reader. Then the cellular iodide uptake by CFTR was initiated by injection of 100  $\mu\text{l}$  NaI buffer (137 mM NaI, 2.7 mM KI, 1.7 mM  $\text{KH}_2\text{PO}_4$ , 10.1 mM  $\text{Na}_2\text{HPO}_4$ , 5 mM D-glucose) into the well with a speed of 150  $\mu\text{l/s}$ , resulting in a final volume of 200  $\mu\text{l}$  (Figure 3.3A). The YFP fluorescence intensity was measured at 485 nm and 530 nm excitation and emission wavelengths, respectively. The potentiators' ability to enhance CFTR channel function was quantified as 1 minus the ratio of fluorescence about 7 seconds after the addition of NaI (F) to the fluorescence before the addition of NaI ( $F_0$ ),  $1 - (\frac{F}{F_0})$ .

An example of YFP iodide quenching is shown as a function K014X potentiator concentration in the presence of 2  $\mu\text{M}$  VX-445 (Figure 3.3B). The rates of iodide influx were determined by linear regression analysis of the initial fluorescence quenching between 1-7s after iodide addition (Figure 3.3C).

### **3.5 Statistical analysis**

Microsoft Excel, OriginLab2015, and XLfit were used to conduct the statistical analyses. Unless otherwise stated, data are reported as mean  $\pm$  SEM or  $\pm$  SDM (standard error or deviation

of the mean) from the indicated number (n) of experiments. Short-circuit current measurements and YFP quenching rate were analyzed using a two-tailed Student's t-test with the means of at least three independent experiments, and the 95% confidence level was considered significant. Statistical significance (P) is indicated \* < 0.05; \*\* < 0.01; \*\*\* < 0.001. The EC<sub>50</sub> values of potentiator compounds were calculated using the OriginLab (Pro) 2015 software by fitting for

$$y = A_1 + \frac{(A_2 - A_1)}{(1 + 10^{((\text{LOG}x - \text{LOG}x_0) * p)})}$$

equation, where A<sub>1</sub> is the value at no addition of the compounds, A<sub>2</sub> is the value at the highest concentration of the compounds, LOG<sub>x0</sub> is the center, and the p is hill slope.

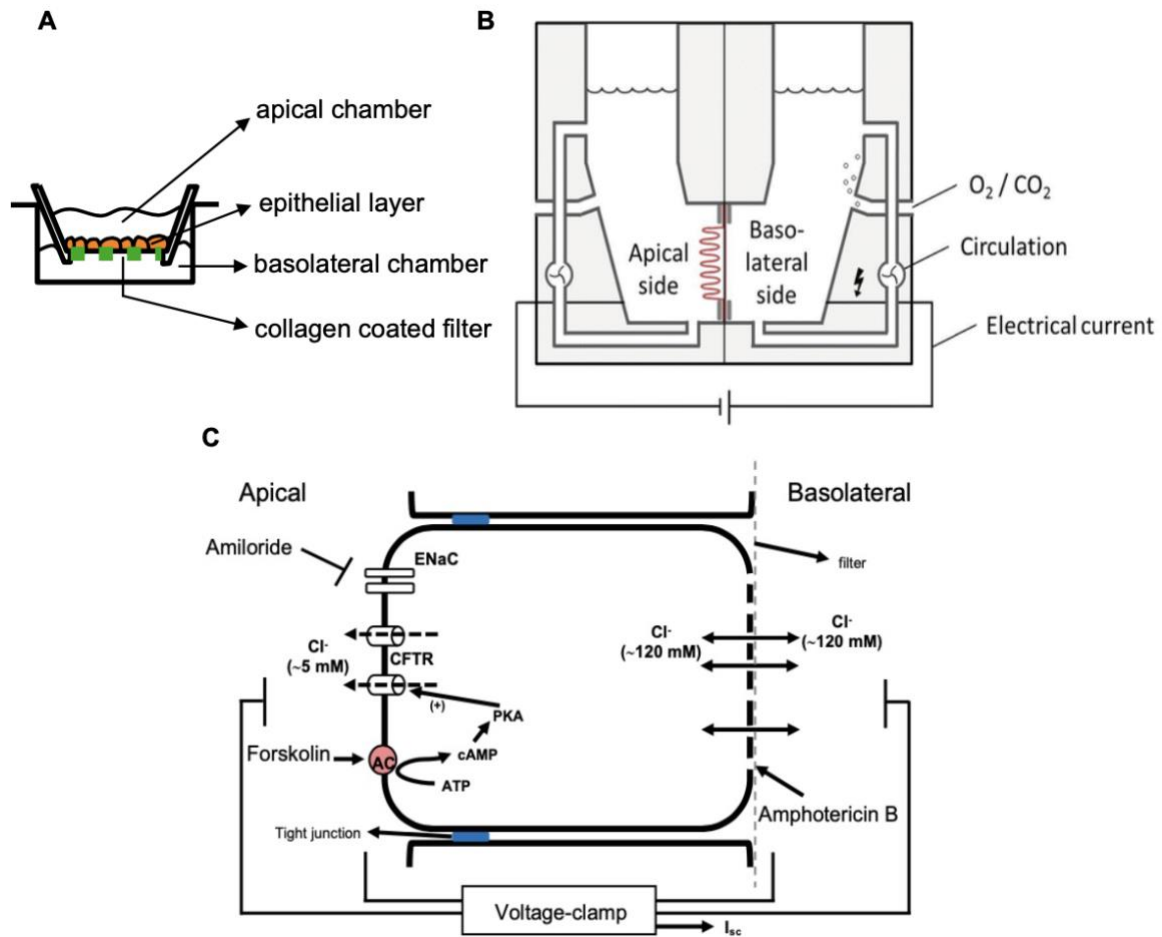


**Figure 3.1. CFTR short-circuit current recording on cultured CFBE41o- monolayer in Ussing Chamber. A) Schematic of cells on snap filter. B) Schematic representation of an epithelial tissue mounted in the Ussing chamber [96]. C) Schematic of Ussing chamber setup (modified from [97]).**

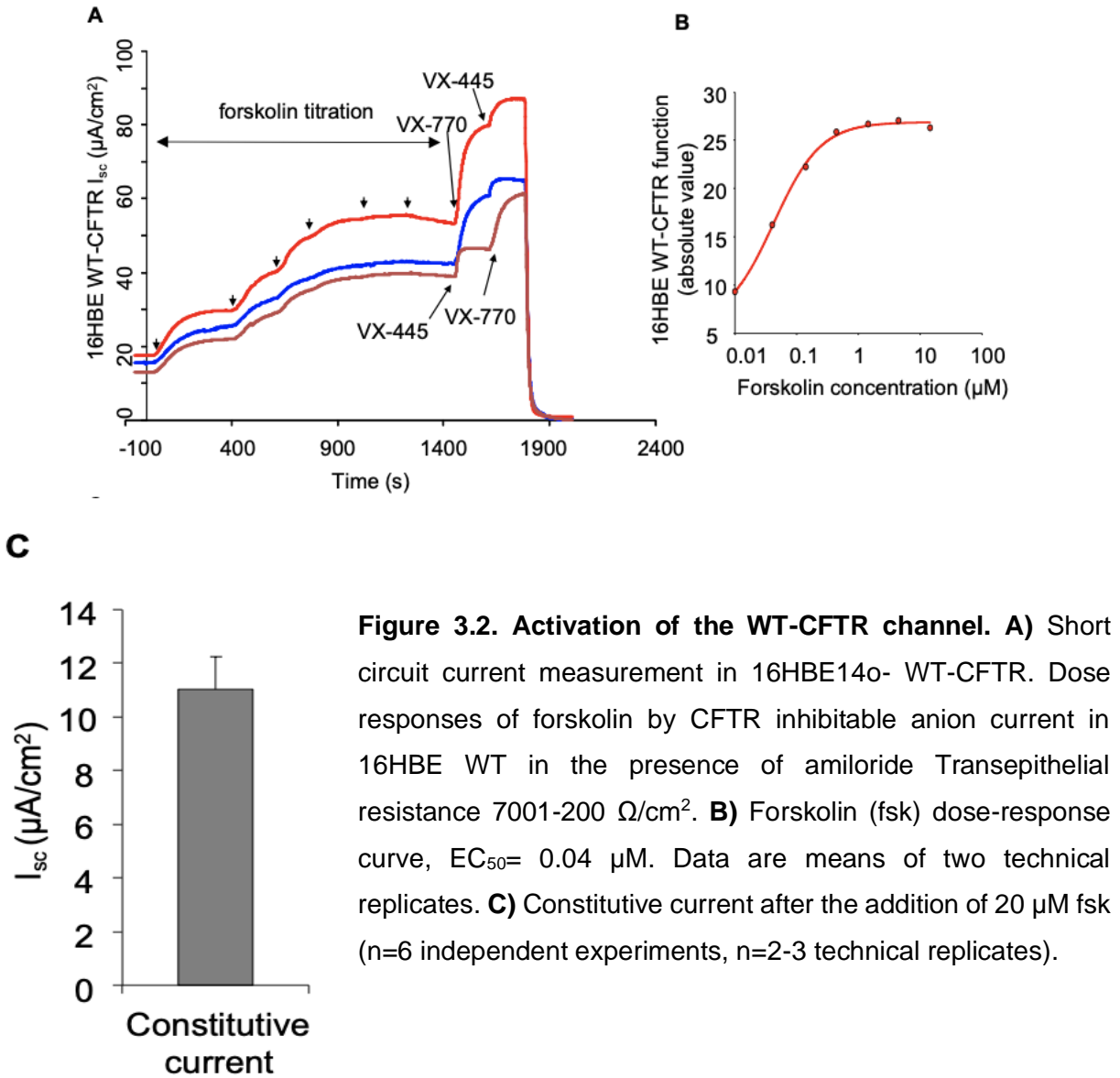


**Figure 3.2. Activation of the WT-CFTR channel.** **A)** Short circuit current measurement in 16HBE14o- WT-CFTR. Dose responses of forskolin by CFTR inhibitable anion current in 16HBE WT in the presence of amiloride Trans epithelial resistance 7001-200  $\Omega/\text{cm}^2$ . **B)** Forskolin (fsk) dose-response curve,  $EC_{50} = 0.04 \mu\text{M}$ . Data are means of two technical replicates. **C)** Constitutive current after the addition of 20  $\mu\text{M}$  fsk (n=6 independent experiments, n=2-3 technical replicates).

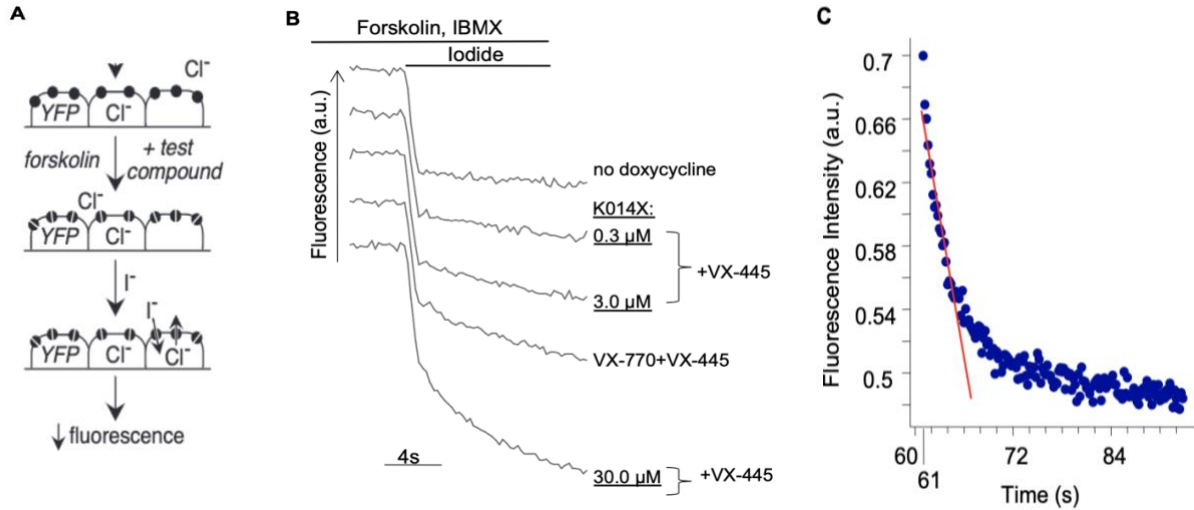


**Figure 3.3. The halide-sensitive Yellow Fluorescence Protein (YFP) quenching assay to measure CFTR-dependent chloride transport activity in the medium-throughput screening assay. A)** CFBE41o- bronchial epithelial cell lines, co-expressing a CFTR variant and the YFP-H148Q/I152L were grown at confluence for 4 days in 96-well plates. Test compounds (CFTR potentiator) and forskolin were added and then YFP fluorescence quenching was initiated by iodide addition. **B)** Time courses of YFP fluorescence intensity changes in CFBE41o- expressing the G551D-CFTR cells under the control of TetOn transactivator. No doxycycline: negative control; 3  $\mu\text{M}$  VX-770+ 2  $\mu\text{M}$  VX-445, positive control alone and in the presence of one of the hit compounds (K014X) at the indicated concentration. **C)** Higher time resolution of the fluorescence quenching kinetics after 60s of PKA activation. Following an instantaneous fluorescence quenching artifact due to the extracellular volume dilution which contains leaked YFP, the initial fluorescence quenching rate (red fitting) was determined by the best linear fitting of the fluorescence intensity decay using the XLfit program, between 61-67s time interval. All individual experiments include n=3-4 technical replicates.

## **Chapter 4: Results**

## **4.1 identification of novel co-potentiators of CFTR gating mutants with improved potency and efficacy**

Our laboratory has recently identified a new CFTR corrector molecule, 4172, that is additive to VX-809 or VX-661, as well as the investigational aminothiazole corrector 3151, in combination resulting in >50% of wild type-level correction of F508del-CFTR [79]. 4172 also displayed limited acute potentiation of WT- and mutant CFTR channel function, which hinted that analogs of this compound may be developed to harbor improved potentiator efficacy and potency [83]. Based on previous observations discussed in the Introduction, we hypothesized that 4172 analogs may have a distinct potentiator mechanism of action (MOA) from that of VX-770 (class I) and VX-445 (class III) potentiators. We received a series of 72 K analogs of the 4172 compound from our collaborator Dr. G. Marzaro (Pharmaceutical and Pharmacological Sciences, Padua University). To test our hypothesis, the potentiator activity of these compounds was determined in the presence of maximally effective concentrations of VX-770 or VX-445 potentiator on CFTR variants with severe gating defects. In addition, the rank order of the 4172 small molecule analogs' efficacy and potency as co-potentiators was established.

### **4.1.1 Screening of the 4172 analogs for G551D-CFTR and N1303K-CFTR co-potentiator activity in CFBE41o- cells**

To characterize the co-potentiator activity of the 4172 analogs with VX-770 or VX-445, we used CFBE41o- cell lines, harboring the inducible expression of the archetypal gating mutant G551D-CFTR, or the N1303K-CFTR severe folding and gating mutant, which have been shown to be responsive to co-potentiators [41]. The CFBE41o- cell lines co-expressed the halide-sensitive YFP, which allowed us to establish the relative efficacy of potentiators on CFTR variants function in a medium-throughput assay [89].

For primary screens for additivity action, the 4172 analog effect was measured at a concentration of 10  $\mu$ M in the presence of saturating concentrations of either VX-770 (3  $\mu$ M) or

VX-445 (2  $\mu$ M) (Figure 4.1). N1303K-CFTR expressing cells were treated with the corrector VX-661 (3  $\mu$ M, 24h, 37°C) before the assay.

The WT-CFTR CFBE14o- cells were induced with 50 ng/ml doxycycline, while the G551D- and N1303K-CFTR cells were induced with 50-250 ng/ml. The background PM chloride permeability was determined in the absence of induction (-dox), i.e., in cells with virtually no CFTR expression. Figures 4.1A-B illustrate the time-dependent YFP-quenching kinetics in the presence of the activated WT- and G551D-CFTR. Following an instantaneous reduction of the fluorescence signal intensity due to the quenching and dilution of the extracellularly leaked YFP, a progressive reduction of fluorescence intensity was observed in the forskolin stimulation WT-CFTR cells. (Figure 4.1A) The progressively increasing iodide-induced quenching can be attributed to CFTR-dependent iodide entry into the cytoplasm because i) CFTR inhibition with the specific CFTR<sub>inh</sub>-172 blocker, as well as ii) the lack of doxycycline induction of CFTR expression, or iii) omitting the CFTR activation by forskolin (Fsk), were able to abolish the progressively increasing intracellular YFP quenching (Figure 4.1A).

Figure 4.1B shows the activation of G551D-CFTR by single or double potentiation. When 4172 analogs, K052X or K084X, were added in combination with VX-770 or VX-445 potentiators, an increase in the G551D-CFTR-dependent quenching rate was observable, indicating an additive activation as compared to that elicited by VX-770 alone (Figure 4.1B).

I screened seventy-two 4172 analogs by measuring the functional rescue of the G551D-CFTR (C) or N1303K-CFTR activity (D) expressed in CFBE41o- YFP cells. The activity of the double potentiators was expressed as the % of the fluorescence quenching rate, measured in the presence upon activation of the G551D-CFTR (4.1C) or N1303K-CFTR (4.1D) in the presence of triple potentiator, VX-770 + VX-445 + apigenin. The most efficacious compounds were chosen for further validation. 6 of 4172 analogs (K014, 52, 64, 70, 71, 84X) were identified as the best hit compounds for G551D-CFTR and 9 analogs for the N1303K-CFTR (K014, 52, 53, 61, 62, 64 70, 71, 73X). The cut-off points for hit selection were chosen arbitrarily at 70% of triple potentiation

(VX-770+VX-445+apigenin) when the analogs were added in combination with 3  $\mu$ M VX-770 (X-axis) or 2  $\mu$ M VX-445 (Y-axis). The arbitrary cut-off points for N1303K-CFTR were 80% of the triple potentiation when the compound was used in combination with VX-770 and 20% in combination with VX-445. Notably, a handful of compounds in combination with VX-770 was able to supersede the VX-770+VX-445+apigenin-provoked N1303K-CFTR channel activation.

#### **4.1.2 Characterization of the best co-potentiators in the presence of FDA-approved potentiators VX-770 or VX-445**

To prioritize the most efficacious 4172 analogs, we measured their potency alone and in combination with VX-770 or VX-445. We assessed the analogs'  $EC_{50}$  for G551D-CFTR potentiation utilizing the halide-sensitive YFP quenching assay by expressing their activity in relation to that measured in the presence of VX-770 and VX-445 (Figure 4.2). The  $EC_{50}$  values are summarized in Table 4.1. Compounds K071X, K070X, and K064X, K084X, K052X, K014X were the most potent respectively, from highest to lowest, either alone or in combination with VX-770 and VX-445. Except for K084X, the observed dose responses of K014X, K052X, K064X, K070X and K071X also confirm the additivity between these compounds and VX-770 or VX-445, consistent with the inference that the analogs may target a distinct, previously unidentified binding site in CFTR (Figure 4.2).

Dose-response measurements of the compounds alone and in combination with VX-770 or VX-445 can also be utilized to gain mechanistic insights. We have shown that the presence of VX-770 increases the potentiator efficacy of VX-445 [63]. This could suggest either VX-770 allosteric influence on the VX-445 binding site conformation or allosteric pathways that are responsible for the G551D-CFTR channel opening [63]. VX-770-mediated alteration of the VX-445 binding site would likely result in a shift in the VX-445 potency. This, however, was not observed (unpublished observations), suggesting independent binding of VX-770 and VX-445. To perform similar investigations for 4172 analogs, the effects of VX-770 and VX-445 on their potency were determined (Figure 4.2). The presence of either VX-770 or VX-445 reduced the

potency of K014X and K052X but not of K064X, K070X and K071X. Indeed, a substantial increase in the K070X and K071X potency was observed by VX-770, suggesting that the conformational changes of VX-770 or VX-445-binding may lead to alterations in the binding site of some of the 4172 analogs (Figure 4.2 and Table 4.1).

#### **4.1.3 Evidence to support 4172 analogs as class II potentiators**

To gain insight into the mechanism of action of the 4172 analogs, first I assessed whether they share a similar mechanism of action with members of class I, class II, or class III potentiators, using combinatorial profiling and clustering analysis in G551D-CFTR expressing CFBE41o- cells (Figure 4.3) (combination from [63]; Vaccarin. C., 2022 [unpublished]). First, the ratio of the measured effect of dual potentiators compared to the theoretical additivity of the single compound effects was calculated. Using this ratio, a heat map of the combinatorial profiles was created for each potentiator. Each compound was used at its saturating concentrations. Then, by using average linkage analysis and then calculating Euclidean distance, clustering was accomplished. The Euclidean distance is a measurement of the straight-line distance between two points, and it is calculated by the square root of the squared differences between the coordinates of the two points. This analysis reveals three clusters of compounds, i.e., compounds that show a similar combinatorial profile, suggesting that there are at least three mechanistic classes of potentiators (combination from [63]; Vaccarin. C., 2022 [unpublished]). The 4172 analogs K014X, K005X, and K019X clustered together with apigenin and bDMC, suggesting that they belong to the same category of class II potentiators (Figure 4.3). The inference from the combinatorial profiling and clustering analysis is supported by manual inspection of the compound effects: For instance, VX-770 is redundant to the Galapagos (GLPG) potentiator, but additive to all other investigated potentiators; concluding that they can be classified as the same class I. Similarly, K014X, K005X, and K019X show no additivity to bDMC or apigenin, class II potentiators; therefore, 4172 analog compounds show a class II potentiator mechanism (Figure 4.3).

To test the validity of the cluster analysis, next, I investigated whether the additivity of all three potentiator classes could be achieved. To this end, we utilized a cell model with endogenous G551D-CFTR expression. The bronchial epithelial cell line 16HBE14o- (16HBE) was modified by CRISPR/Cas9 gene-editing (ge) to contain a single copy of the G551D-CFTR. It has been described and was kindly provided by the Cystic Fibrosis Foundation Therapeutics (CFFT) [98]. 16HBEge cells were polarized on permeable filter supports and the G551D-CFTR function was determined by short-circuit current ( $I_{sc}$ ) measurement. Consistent with its severe gating defect, G551D-CFTR showed only minimal response to forskolin-induced activation of the PKA (Figure 4.4). Since VX-770 is a permissive factor for VX-445 potentiation [63], this potentiator was added first, followed by the subsequent addition of VX-445 and apigenin as second and third potentiators, respectively (Figure 4.4).

Each of the potentiators, VX-770, VX-445 and apigenin, individually increased the G551D-CFTR function, with contributions of ~27%, ~40%, and ~28% to the maximal  $I_{sc}$ , respectively (Figure 4.4). The order of addition of the second and third potentiator did not affect the maximal current, which reached ~185% of that of forskolin-activated WT-CFTR in parental 16HBE cells, which also contains a single copy of the WT-CFTR gene. These results support the additive effects of potentiators from the three classes, which as a triple combination mediate increased channel function.

#### **4.1.4 Potency and efficacy of VX-770, VX-445 and 4172 analog-mediated triple potentiation of G551D-CFTR**

To replicate triple potentiation results using 4172 analogs, short circuit current ( $I_{sc}$ ) measurements in an Ussing chamber setup were performed in G551D-CFTR expressing 16HBE14o- cells. The  $I_{sc}$  was measured in the presence of forskolin (20  $\mu$ M), and the specificity of the currents was confirmed by the addition of the CFTR<sub>inh</sub>-172 at the end of the experiment (Figure 4.5A). The potentiators 3  $\mu$ M VX-770, 2  $\mu$ M VX-445 and 10  $\mu$ M K014X were consecutively added to the apical side of the epithelial cells. Acute addition of 10  $\mu$ M K014X as the third

potentiator resulted in a  $\sim 8 \mu\text{A}/\text{cm}^2$  increase in  $I_{\text{sc}}$ , approximately 20% of the total CFTR-mediated  $I_{\text{sc}}$  ( $\sim 50 \mu\text{A}/\text{cm}^2$ ) (Figure 4.5A, B). Reversing the addition order of VX-445 and K014X yielded similar results. The fully potentiated 16HBE G551D-CFTR channel showed an  $I_{\text{sc}}$  of approximately  $50 \mu\text{A}/\text{cm}^2$ , corresponding to 85% of forskolin-activated WT-CFTR (Figure 4.5B)

To further investigate the efficacy and potency of a 4172 analog as the third potentiator, a dose-response of K052X in the presence and absence of VX-770+VX-445 was performed using the halide-sensitive YFP quenching assay and YFP+G551D-CFTR expressing CFBE41o- cells (Figure 4.6). K052X increased the phosphorylated G551D-CFTR function to  $\sim 115\%$  of that achieved by VX-770+VX-445 potentiation. The addition of K052X as a third potentiator increased the VX-770+VX445 potentiated G551D function to  $\sim 200\%$ , indicating a 25% higher efficacy of K052X in comparison to  $50 \mu\text{M}$  Apigenin as a third potentiator. The potency of K052X increased when the K052X was added in combination with VX-770+VX-445, significantly decreasing the  $\text{EC}_{50}$  value from  $25.9 \pm 1.4 \mu\text{M}$  to  $5.5 \pm 17.1 \mu\text{M}$ . Data are means  $\pm$  SEM of three independent measurements.

#### **4.1.5 Functional correction of N1303K-CFTR by triple potentiators in 16HBE14o- and primary primary human nasal epithelia (HNE) cells**

To analyze the hit compounds obtained in 4.1.2. section for their efficacy and potency as third potentiators for VX-661 corrected N1303K-CFTR, short circuit current ( $I_{\text{sc}}$ ) measurements were performed in an Ussing chamber setup. The  $I_{\text{sc}}$  was measured in the presence of forskolin ( $20 \mu\text{M}$ ), and the specificity of the currents was confirmed by the addition of the CFTR<sub>inh</sub>-172 at the end of the experiment (Figure 4.7A). The three potentiators  $3 \mu\text{M}$  VX-770,  $2 \mu\text{M}$  VX-445 and increasing concentrations of 4172 analogs were consecutively added to the apical side of the epithelial cells. The quantification of the contribution of individual potentiators to the phosphorylated N1303K-CFTR current is shown in Figure 4.7B-C. The VX-770+VX-445 combination produced a channel function in 16HBE cells that was approximately 40% of that of forskolin-activated WT-CFTR. When 4172 analogs were added, the channel function was

significantly further enhanced by 14–26% of the WT current, reaching ~60-80% of the WT current, i.e., a channel function that would likely result in a clinical benefit (Figure 4.7D). The EC<sub>50</sub> of K014X, K052X, K064X, K070X, and K084X were 1.6 μM, 0.75 μM, 3.1 μM, 2.6 μM, and 2.6 μM respectively, thus in a range that may support drug development (Figure 4.7B-C).

Similar results were obtained in primary human nasal epithelia (HNE), which were isolated from a patient homozygous for the N1303K mutation and differentiated for three weeks at the air-liquid interface. Potentiation of VX-661-corrected and phosphorylated N1303K-CFTR with VX-770+VX-445 resulted in a current corresponding to 19% of the average forskolin-stimulated WT-CFTR current in HNE from 10 donors (Figure 4.8). 4172 analogs enhanced the channel function by 10–15% of the WT current, resulting in a current of up to 36% for the combination of VX-770+VX-445+K052X (Figure 4.8B), a level that would likely translate to a significant clinical benefit. In both cell models, the 16HBE cell line and primary HNE, the compound K052X in combination with VX-770+VX-445 provided the highest efficacy of functional channel correction.

#### **4.1.6 The addition of a third potentiator increases the functional correction efficacy of some rare CF mutants.**

The CFTR modulator drug Trikafta, containing VX-661, VX-445 and VX-770, has recently been FDA-approved for additional >170 CFTR mutants by label extension. However, many of these mutants are incompletely corrected by the Trikafta therapy [99], which may in part be due to an incompletely restored gating phenotype. Thus, the introduction of a third potentiator may increase the clinical benefit of Trikafta therapy for some patients. As a proof of principle, we tested the top 4172 analog hits as third potentiators on other mutations such as S549R- and S549N-CFTR utilizing the halide-sensitive YFP quenching assay (Figure 4.9). Figure 4.9A indicates analog curves of the YFP iodide quenching rate in S549R-CFTR expressing CFBE41o- cells. Since the S549R-CFTR variant is not only a gating mutation but also a folding mutation, the cells were treated with the corrector VX-661 for 24 hours. The triple potentiation with VX-770+VX-445

+ 4172 analogs, except K014X, significantly increased the channel function in comparison to VX-770+VX-445 potentiation (Figure 4.9B).

In contrast, the gating mutant S549N-CFTR does not exhibit a folding defect hence, VX-661 conferred no additional benefit (Figure S.1). While S549N was highly responsive to potentiation with VX-770+VX-445 in the halide-sensitive YFP quenching assay, this mutant was not responsive to the addition of a third potentiator (Figure S.2).

## **4.2 Mechanistic understanding of novel potentiators**

The methods by which these novel potentiators interact with the mutant CFTR protein to restore its activity were investigated next. This knowledge can help to better understand the gating mechanism of CFTR in the presence of potentiators and determine drug-drug interactions, which may improve future efforts in drug design.

### **4.2.1 The impact of VX-661 on the efficacy and potency of the 4172 analog potentiators**

Recently, it was suggested that type I correctors with clinical approval, such as VX-661 (Tezacaftor) bind within MSD1 and either co-translationally [100] or post-translationally [77] inhibits misfolding, which improves the plasma membrane expression (PME) of some misfolded CFTR variants. Soya et al. also showed that VX-809, an analog of the VX-661, binding to the MSD1 can allosterically stabilizes the MSD2 [77], which may alter the potentiator rescue effect. To test whether the correction of CFTR folding mutations has any impact on the efficacy and potency of 4172 analog potentiators, the dose-response of K064X and K070X for the potentiation of N1303K-CFTR expressing 16HBE14o- with or without VX-661 correction was determined by  $I_{sc}$  measurement (Figure 4.10A). Surprisingly, VX-661 correction decreased the efficacy of K064X and K070X despite the increased availability of the corrected protein at the plasma membrane. VX-661 also decreased the potency of K064X and K070X when applied as a triple combination with 3  $\mu$ M VX-770 + 2  $\mu$ M VX-445. The  $EC_{50}$  values were increased from  $1.0 \pm 0.3 \mu$ M to  $2.6 \pm 0.1 \mu$ M for the K070X, and from  $1.5 \pm 0.3 \mu$ M to  $3.1 \pm 0.7 \mu$ M for the K064X compound. Similar

measurements were performed for the S549R-CFTR mutation. The dose-response of K052X in CFBE410- S549R-CFTR cells in the presence or absence of VX-770+VX-445, with or without VX-661 correction was determined in halide-sensitive YFP quenching assays (Figure 4.10B). The 4172 analogs' efficacy and potency (e.g., K052X) were not significantly influenced by the maximal VX-661 correction. However, the efficacy of K compounds alone or as a triple potentiator combination was increased by VX-661 correction. These experiments suggest mutation-specific drug-drug interactions, consistent with long-range inter-domain dynamic backbone and side allosteric coupling in the CFTR [77].

#### **4.2.2 Does the co-potentiator activity require CFTR phosphorylation?**

An essential step for CFTR canonical activation is the channel PKA-dependent phosphorylation. As was explained in the introduction, the CFTR chloride channel's ability to open and close can be regulated by the R domain phosphorylation, which facilitates the displacement of the R domain and the dimerization of the NBDs [78]. To interrogate whether the 4172 analogs require phosphorylation for their potentiator function we conducted assays using the 15SA-CFTR variant, in which 15 serine residues in the PKA consensus sites have been mutated to alanine. The 15SA-CFTR exhibits only ~10% of the WT response upon forskolin-mediated PKA activation [101].

The potentiator combination VX-770+VX-445 elicited a substantial channel function of 15SA-CFTR regardless of forskolin activation (Figure 4.11A and B). The channel function was significantly augmented by apigenin or K052X as third potentiators. To confirm that the 15SA-CFTR current is PKA-mediated phosphorylation independent we inhibited the PKA-inhibitor by H89 ( $EC_{50}$  ~135 nM). H89 did not significantly inhibit the triple potentiator mediated current (Figure 4.11A and B). Taken together, these results suggest that the combination of the three potentiators VX-770+VX-445+K052X is sufficient to elicit iodide conductance independent of CFTR phosphorylation.

To confirm these results using a second technique, which allows quantifying the channel activation in relation to the forskolin-activated WT-current, we performed short circuit current measurements in CFBE41o- 15SA-CFTR cells. A combination of the three classes of potentiators, VX-770, VX-445 and apigenin, was able to increase the function of CFTR-15SA to ~80% of the forskolin-stimulated WT-CFTR activity both in the presence and absence of H89 PKA-inhibition (Figure 4.11C and D), confirming that PKA-dependent phosphorylation is not a prerequisite for triple potentiator-mediated channel activation.

To further validate these results, we tested the phosphorylation independence of 4172 analogs as third potentiators in other mutations such as G551D- and N1303K-CFTR, using the halide-sensitive YFP quenching assay (Figure 4.12). As before, the addition of VX-770+VX-445 resulted in the channel function of VX-661 corrected N1303K-CFTR and G551D-CFTR in the presence of forskolin, which was further augmented by the addition of third potentiators, both apigenin and 4172 analogs. Importantly, in the absence of PKA activation with forskolin, we observed similar channel activation by potentiator combinations, suggesting that the R domain phosphorylation is dispensable for CFTR activation by potentiator combinations (Figure 4.12).

#### **4.2.3 Is NBD-dimerization required for CFTR variant activation by double or triple potentiation?**

To test whether the triple potentiation by the 4172 analogs is NBD-dimerization dependent, we used the CFBE41o- cells that express the C-terminally truncated CFTR variant W1282X that lacks ~60% of the NBD2 domain [37]. Despite the lack of functional NBD dimer formation, the addition of VX-770+VX-445 elicited some channel activity that was significantly increased by the addition of 4172 analogs as the third potentiator (Figure 4.13). Since W1282X-CFTR is associated with a folding defect and the channel expression is partly restored by the VX-661 correction [37], we repeated the experiment after the VX-661 treatment. Unsurprisingly, this led to an increased channel function in the presence of potentiator combinations. Taken together, this experiment

suggests that canonical NBD dimerization is not required for the 4172 analog potentiator function in combination with VX-770+VX-445.

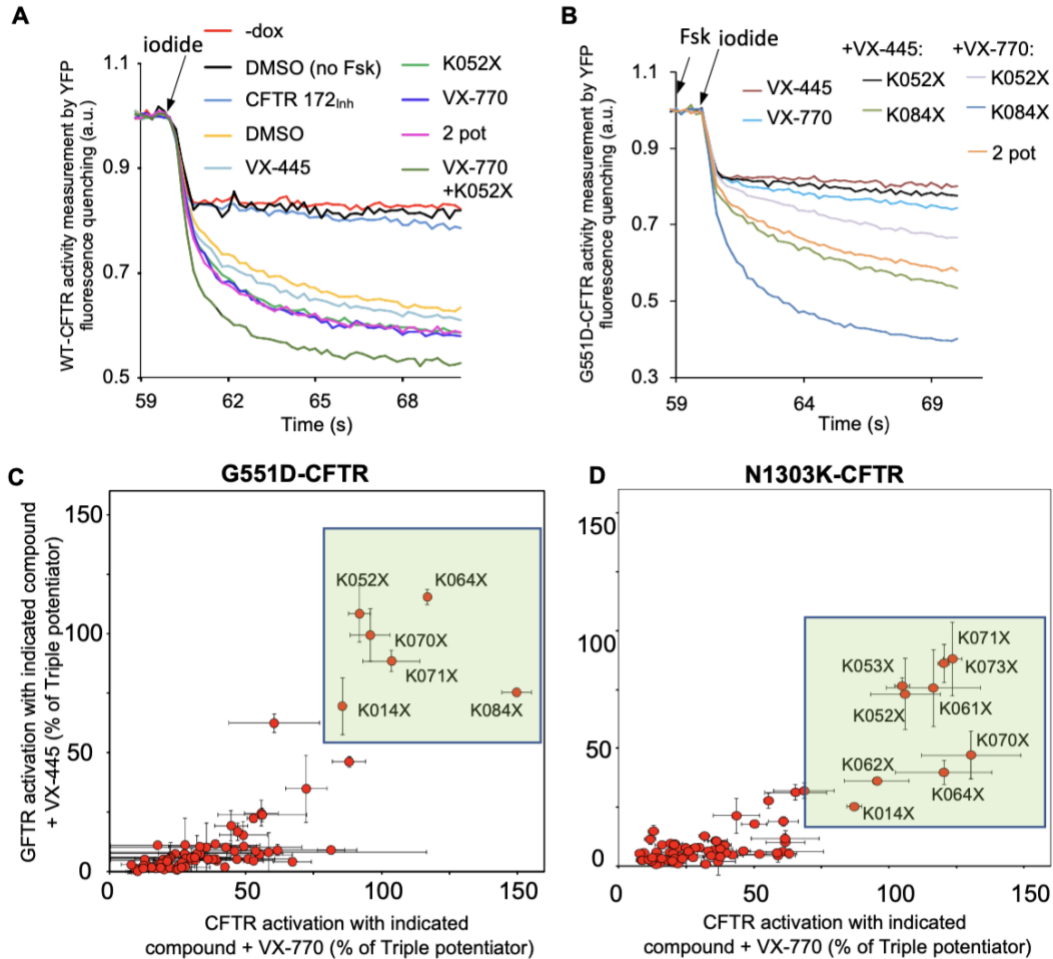


**Figure 4.1. Characterization of 4172 analogs as co-potentiators of the phosphorylated CFTR variants by the halide-sensitive fluorescence quenching assay in CFBE41o- cells.** All measurement was done with phosphorylated CFTR. **A-B)** Iodide quenching curves of forskolin-induced phosphorylated WT-CFTR (**A**) and G551D-CFTR (**B**). The VX-770 (3  $\mu$ M), VX-445 (2  $\mu$ M), and K052X compounds were added acutely, increasing CFTR activity. The fluorescence quenching is CFTR-dependent because the CFTR-specific Inh-172 channel blocker prevented the iodide-induced fluorescence quenching. **C-D)** Primary screen of 4172 analogs as co-potentiator in combination with VX-770 or VX-445 in G551D-CFTR (**C**) or N1303K-CFTR (**D**) expressing CFBE41o- cells. The relative transport activity of CFTR variants was measured by the iodide-sensitive quenching rate of the constitutively expressed halide-sensitive YFP in CFBE41o- cells. The 6 and 9 of the most efficacious (“hit”) compounds from G551D- and N1303K-CFTR screens were selected for further validation. Means  $\pm$  SD are shown (technical replicate n=4; representative of n=5 independent experiments) and **D)** the 9 selected analogs in N1303K-CFTR (technical replicate n=4; n=1). CFBE41o- N1303K-CFTR cells were treated 24h with VX-661. Means  $\pm$  SD are shown. Triple potentiation = 3 $\mu$ M VX-770, 2 $\mu$ M VX-445, and 50 $\mu$ M Apigenin.

### CFBE41o- G551D-CFTR

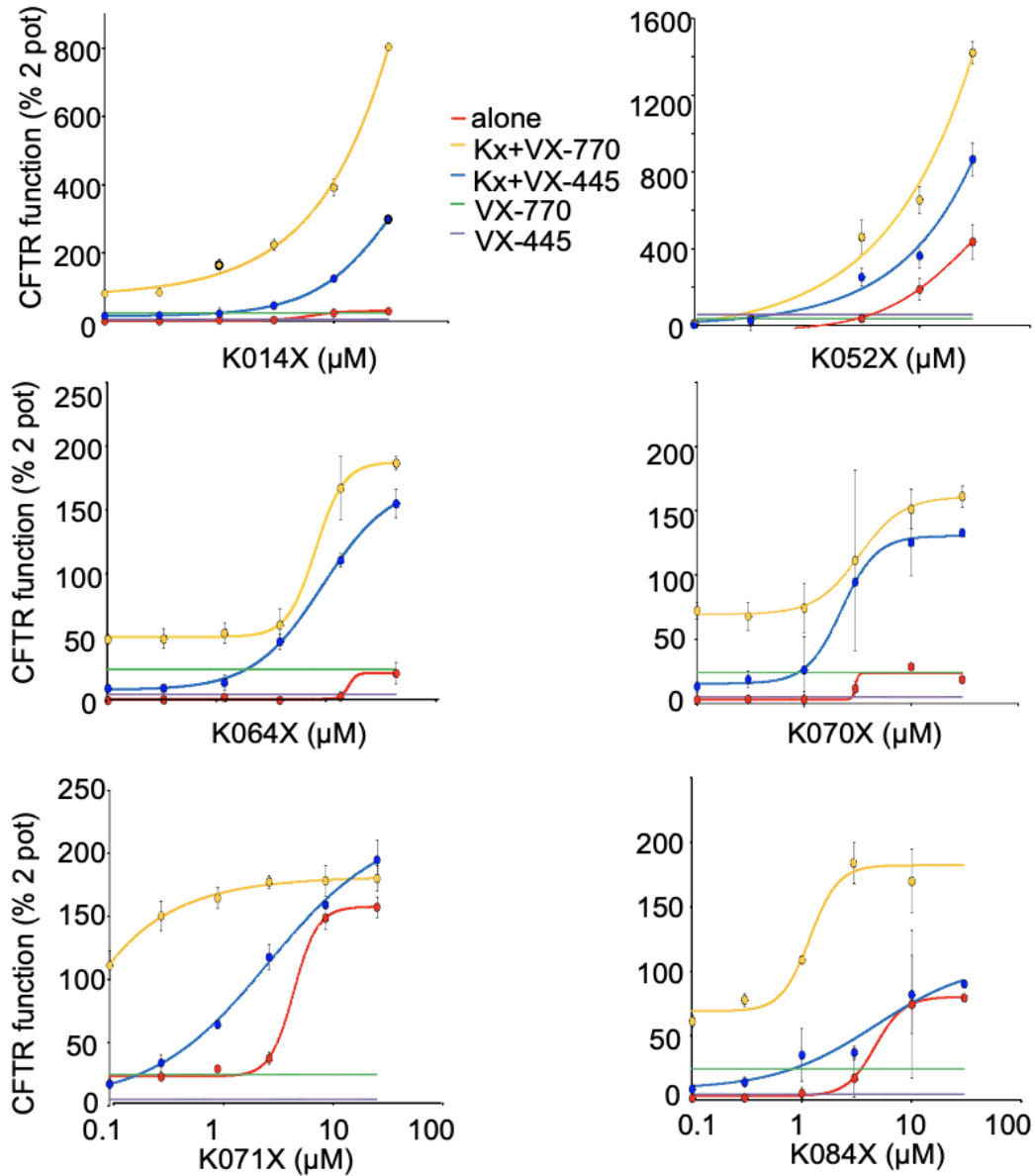


**Figure 4.2. Phosphorylated G551D-CFTR co-potentialion by 4172 analogs in the presence of VX-445 or VX-770.** G551D-CFTR activity relative to that in the presence of 3 μM VX-770 and 2 μM VX-445 was determined by the halide-sensitive YFP assay in CFBE41o-cells. The green and purple line shows G551D-CFTR activity in the presence of 3 μM VX-770 or 2 μM VX-445, respectively, as reference. The EC<sub>50</sub> values are summarized in Table 1.1. The means and standard deviation of four technical replicates are shown of two independent experiments.

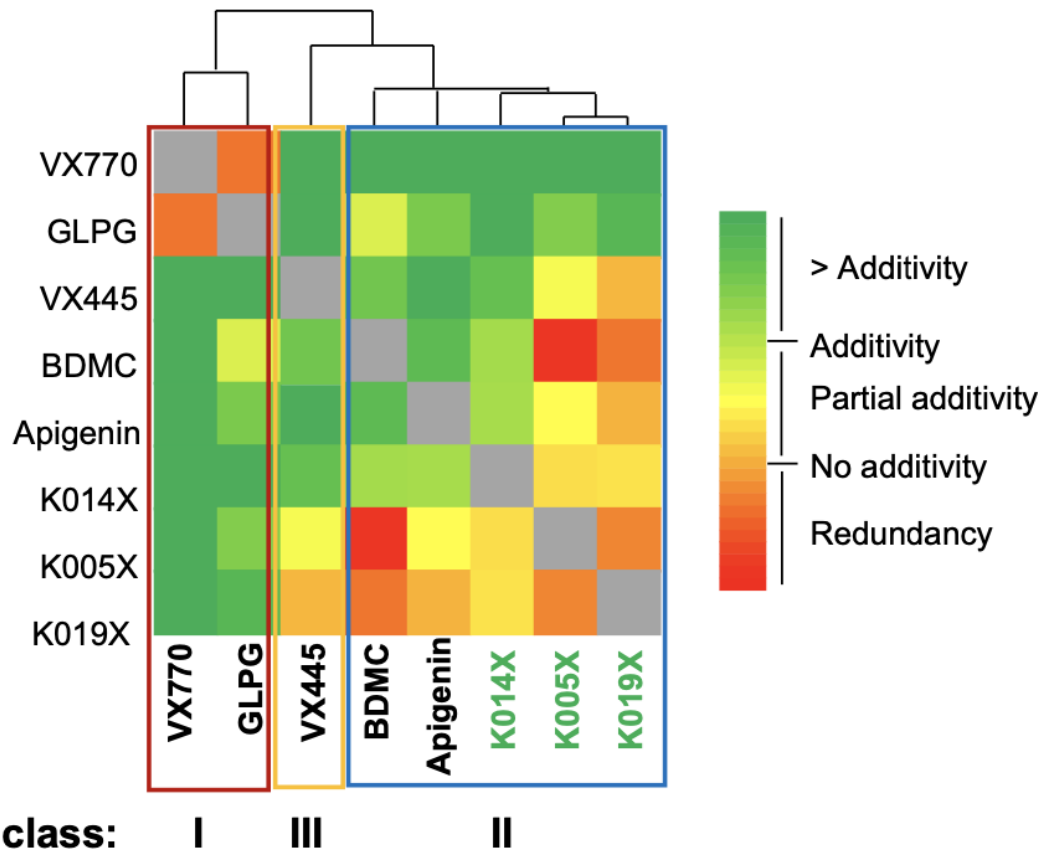


**Figure 4.3. Functional classification of the K0 series 4172 analogs potentiator activity based on their combinatorial cluster analysis using established class I-III potentiators and G551D-CFTR and halide-sensitive YFP expressing in CFBE410o- cells.** A Heatmap of the combinatorial profiling was generated by comparing the dual potentiator effect in relation to their predicted additive activity based on individual potentiator activity at saturating drug concentration, using the halide-sensitive YFP assay and phosphorylated G551D-CFTR. K005X and K014X elicit additive G551D-CFTR activity in concert with Class I or Class III potentiators at saturating compound concentration, consistent with their mechanism of action as Class II potentiators. Data were generated in 3-5 independent experiments, n=4 technical replicates [combination from [63] (permission from Elsevier journal) and Vaccarin. C. unpublished data).

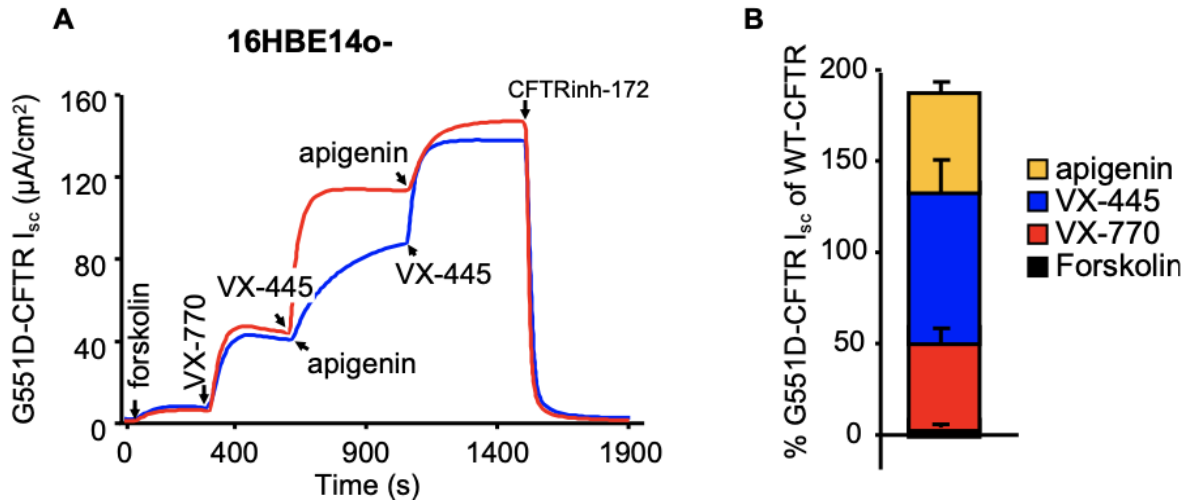


**Figure 4.4. The combination of three classes of potentiators leads to G551D-CFTR hyperactivation relative to the WT-CFTR. A)** Representative  $I_{sc}$  recording of G551D-CFTR in gene-edited (ge) 16HBE14o- cells (16HBEge) activated with forskolin (Fsk, 20  $\mu\text{M}$ ), followed by the indicated order of VX-770 (3  $\mu\text{M}$ ), VX-445 (2  $\mu\text{M}$ ), and Apigenin (50  $\mu\text{M}$ ). CFTR was inhibited with CFTRinh-172 (20  $\mu\text{M}$ ). **B)** Quantification of the G551D-CFTR activity in experiments displayed on panel A. The  $I_{sc}$  magnitude is expressed relative to that of the WT-CFTR in 16HBE cells. Means  $\pm$  SEM,  $n=3$  independent experiments,  $n=3$  technical replicates.

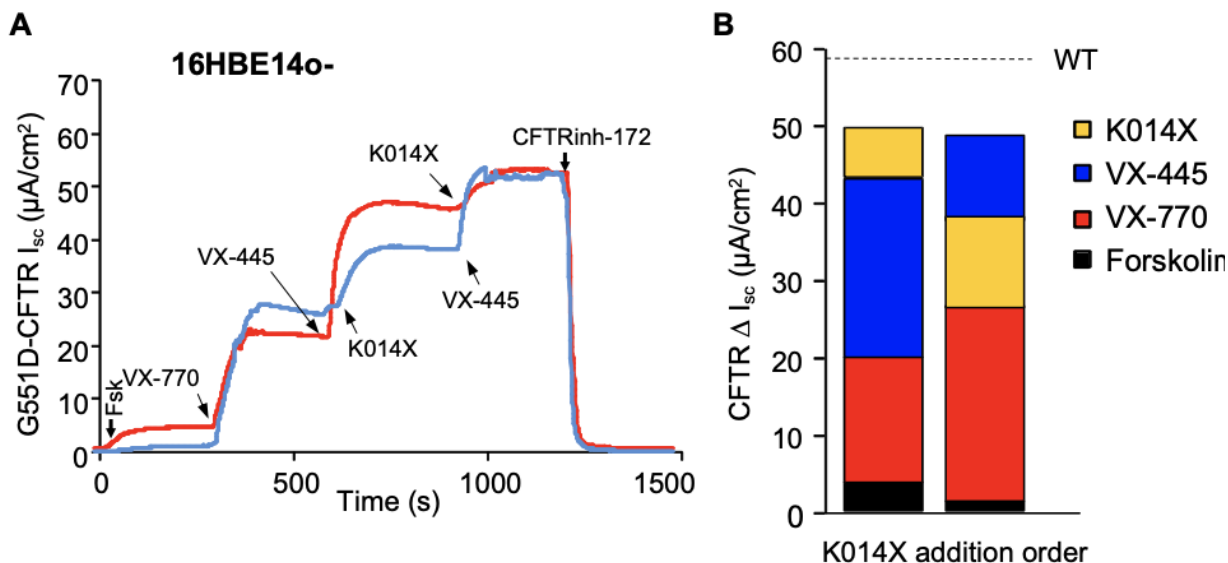


**Figure 4.5. The combination of multiple potentiators leads to the activation of G551D.** **A)** Hit compound K014X as a double or triple potentiator. Representative traces (left) of the  $I_{sc}$  of G551D-CFTR in gene-edited (ge) 16HBE14o- activated with forskolin (Fsk, 20 $\mu\text{M}$ ) and potentiated with VX-770 (3 $\mu\text{M}$ ) followed by VX-445 (2 $\mu\text{M}$ ) and hit compound K014X (10  $\mu\text{M}$ ) or in reverse order. At the end of the experiment, CFTR was inhibited with CFTR<sub>Inh</sub>-172 (20  $\mu\text{M}$ ). **B)** Quantification of the  $I_{sc}$  shows the contribution of Fsk, VX-770, VX-445 and K014X to the maximal current, depending on the order of potentiator addition, in 16HBE14o- cells (technical replicate of n=3, n=1).

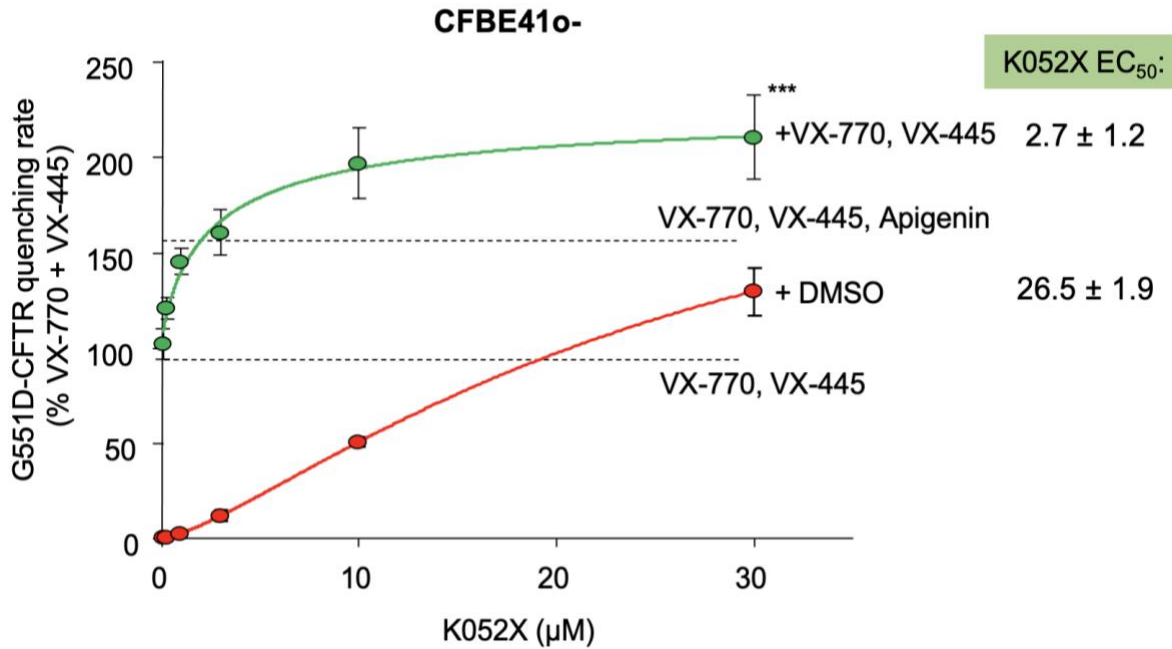


**Figure 4.6. Not only the efficacy but the potency of the K052X (class II) increased by class I and III potentiators in G551D-CFTR expressing CFBE41o- cells.** K052X dose-response curves in the absence (+DMSO) and presence of VX-770 (3 µM) + VX-445 (2 µM) were measured by the halide-sensitive YFP assay in CFBE41o- cells, using a linear fit of the initial decay rate at time point 61-second. The K052X EC<sub>50</sub> was reduced from ~26.5 µM to ~2.7 µM in the presence of VX-770 and VX-445. The legend is described as: 2µM VX-445; 3µM VX-770; 2 pot = VX-445+VX-770; 3 pot= 3µM VX-770+ 2µM VX-445 + 50µM Apigenin; and the triple combination of doses of K052X in addition to 2 pot. The cells were induced with 250 ng/mL doxycycline. Data are means ± SEM of three independent measurements, technical replicate of n=4.

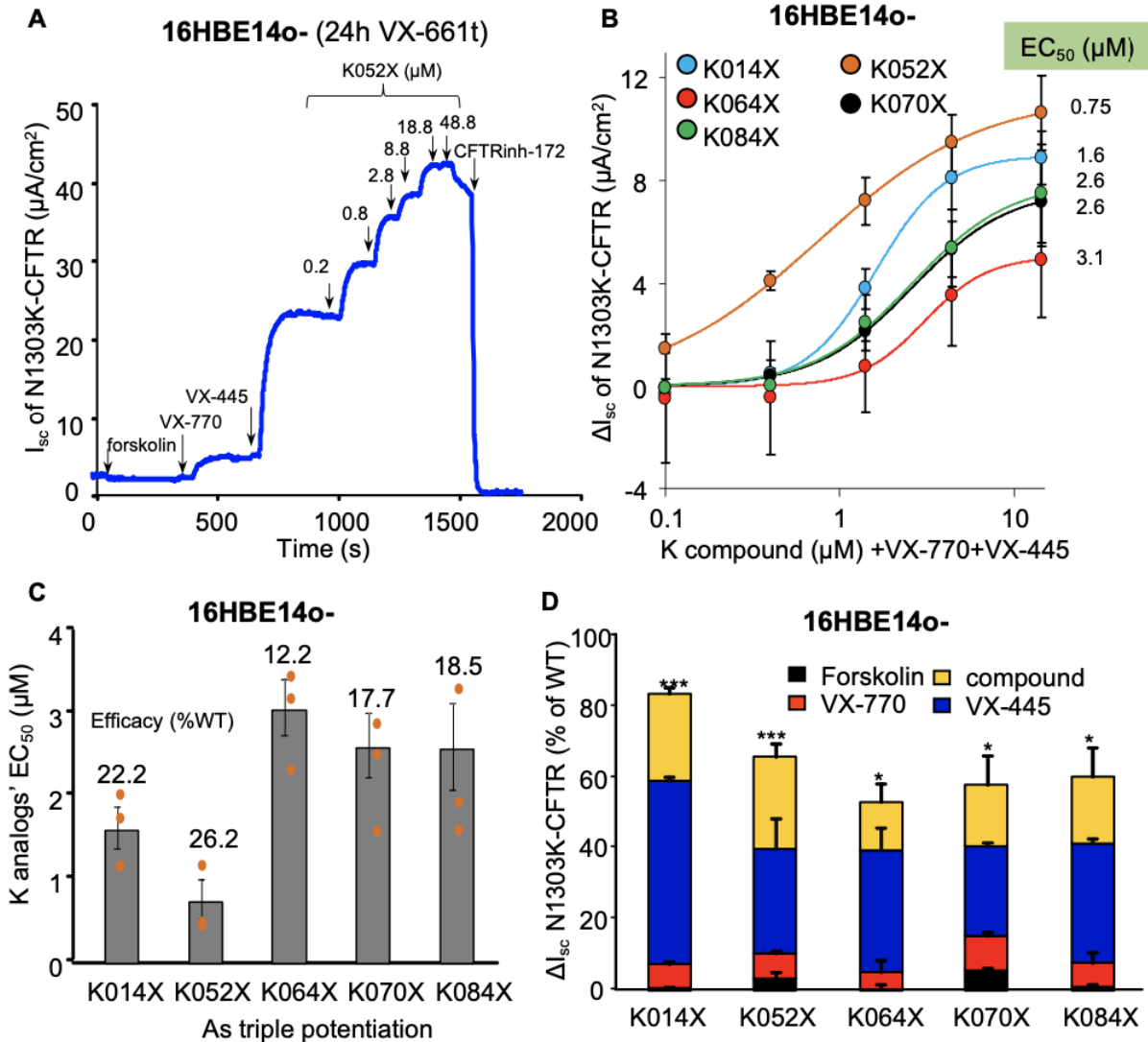


**Figure 4.7. The efficacy and potency of 4172 analogs on the phosphorylated N1303K-CFTR activity in the presence of VX-770 and VX-445.**  $I_{sc}$  measurements were performed on the gene-edited 16HBE14o- cells. **A)** Representative traces of  $I_{sc}$  of N1303K-CFTR activation with forskolin (Fsk, 20  $\mu\text{M}$ ), VX-770 (3  $\mu\text{M}$ ), and VX-445 (2  $\mu\text{M}$ ), followed by increasing concentration of the K052X. **B)** EC<sub>50</sub> determination of the indicated potentiator hits based on  $I_{sc}$  determination as in panel A. The EC<sub>50</sub> of K014X, K052X, K064X, K070X, and K084X are ~1.6, 0.75, 3.1, 2.6, and 2.6  $\mu\text{M}$  respectively, determined by Origin software ( $n=3$ , 2-3 technical replicates). **C)** Efficacy and potency of K analogs, added as triple potentiation with VX-770 and VX-445, in percent of WT-CFTR. **D)** Maximal efficacy of the triple potentiation combination on the N1303K-CFTR activation was expressed relative to the WT-CFTR  $I_{sc}$ . The contribution of individual potentiators to the phosphorylated N1303K-CFTR current activity was measured at their maximally effective potentiator concentration. Data are means  $\pm$  SEM of 3 technical replicates in three independent experiments.

**Table 4.1. Summary of all hit compounds' efficacy and potency.** Co-potential determination in CFBE41o- G551D-CFTR by halide-sensitive YFP assay; technical replicate n=4, representative of n=2 independent experiments. Triple potentiation efficacy and potency determination in 16HBE14o- N1303K-CFTR by short circuit current measurement; technical replicate n=3, n=1-3 independent experiments. Data are obtained from experiments in Figures 4.2 and 4.7.

Compounds	CFBE41o- (YFP)			16HBE14o- ( $I_{sc}$ )		
	Co-potential $EC_{50}$ ( $\mu$ M), G551D-CFTR			Triple potentiation $EC_{50}$ ( $\mu$ M) and Efficacy, N1303K-CFTR		
	Alone	+VX-770	+VX-445	+VX-770, VX-445	Efficacy of triple potentiation (% of WT $I_{sc}$ )	$\Delta$ additivity of compound (% of WT $I_{sc}$ )
K014X	6.3	>30	43.4	1.6	84.1	22.2
K052X	28.5	>30	>30	0.75	66.3	26.2
K064X	11.8	6.1	7	3.1	53.3	12.2
K070X	3.4	3.3	2.3	2.6	58.2	17.7
K071X	1.4	0.4	2.7	-	-	-
K073X	>100	>100	>100	-	-	-
K084X	15.2	0.9	>100	2.6	60.5	18.5

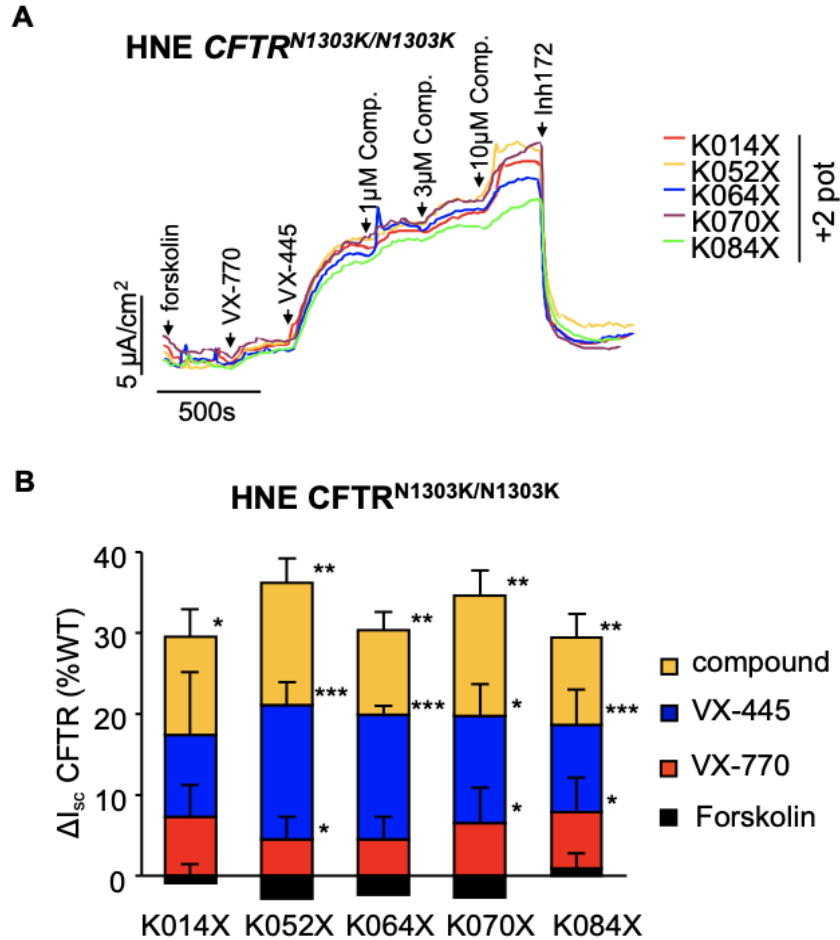


**Figure 4.8. Correction efficacy of triple potentiator combinations on N1303K-CFTR in primary HNE epithelia.** **A)** Representative traces and **B)** quantification of  $I_{sc}$  of VX-661 corrected (3  $\mu\text{M}$ , 24 hours, 37  $^{\circ}\text{C}$ ) N1303K-CFTR activation in homozygous primary HNE monolayers upon activation with forskolin (Fsk, 20  $\mu\text{M}$ ), followed by potentiation with VX-770 (3  $\mu\text{M}$ ), VX-445 (2  $\mu\text{M}$ ), and the indicated 4172 analog hit (14  $\mu\text{M}$ ). Data are means  $\pm$  SD of three measurements ( $n = 3$ ). \* $P < 0.05$ , \*\* $P < 0.01$ , \*\*\* $P < 0.001$  by unpaired two-tailed t-test for the successive addition of potentiators.

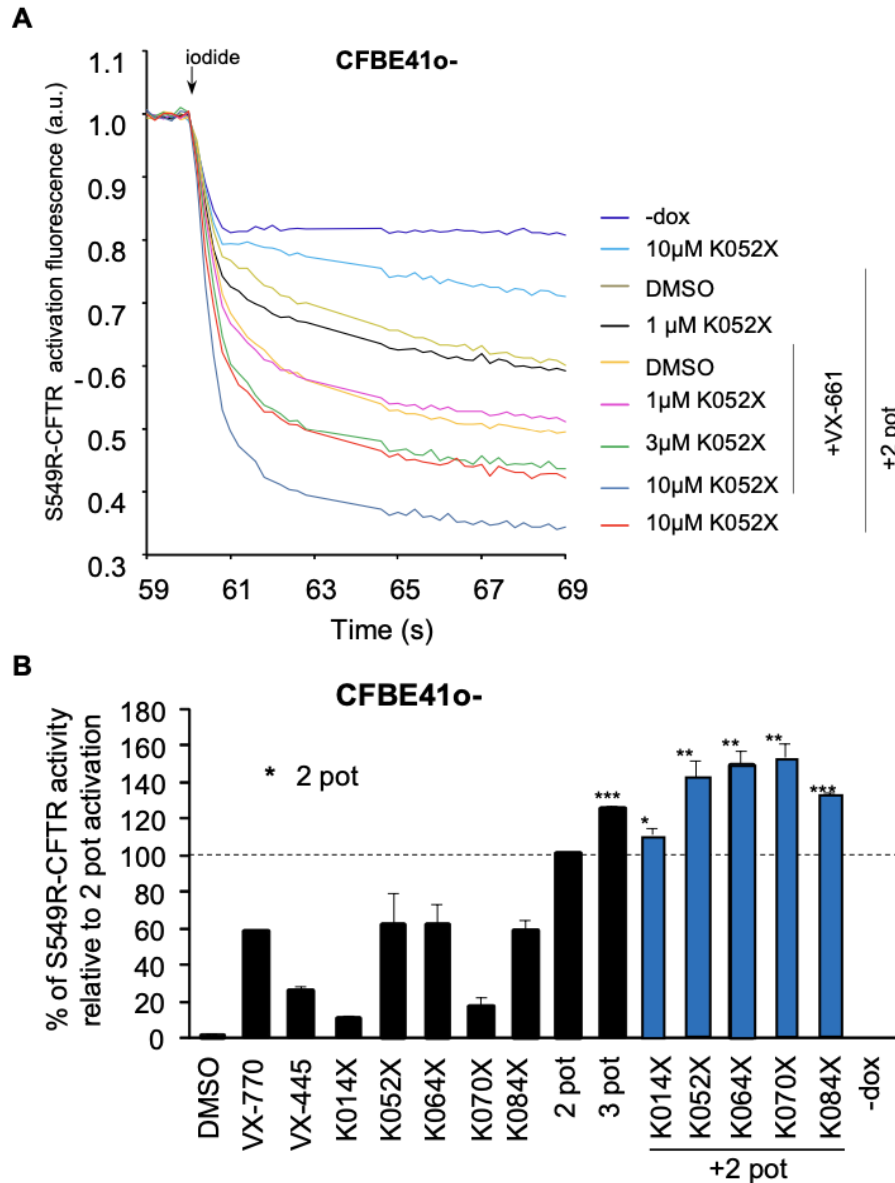


**Figure 4.9. The 4172 co-potentiator analogs augment the phosphorylated S549R-CFTR mutant activity in CFBE41o<sup>-</sup> cells, determined by the halide-sensitive YFP assay. A)** Representative traces of YFP quenching kinetics. The legend is described as: -dox= no doxycycline; 2  $\mu$ M VX-445; 3  $\mu$ M VX-770; 2 pot= VX-445+VX-770; 3 pot= 3  $\mu$ M VX-770+ 2  $\mu$ M VX-445 + 50  $\mu$ M Apigenin; and the triple combination of doses of K052X in addition to 2 pot. **B)** Triple potentiation effects of analogs K014, 52, 64, 70, and 84X (n=3 independent experiment, 4 replicates per experiment; 3  $\mu$ M VX-770 + 2  $\mu$ M VX-445). Cells were induced 4d with 250ng/ml doxycycline and 3 $\mu$ M VX-661 24h at 37°C. Data are means  $\pm$  SEM of three measurements. \* $P$  < 0.05, \*\* $P$  < 0.01, \*\*\* $P$  < 0.001 by unpaired two-tailed t-test.

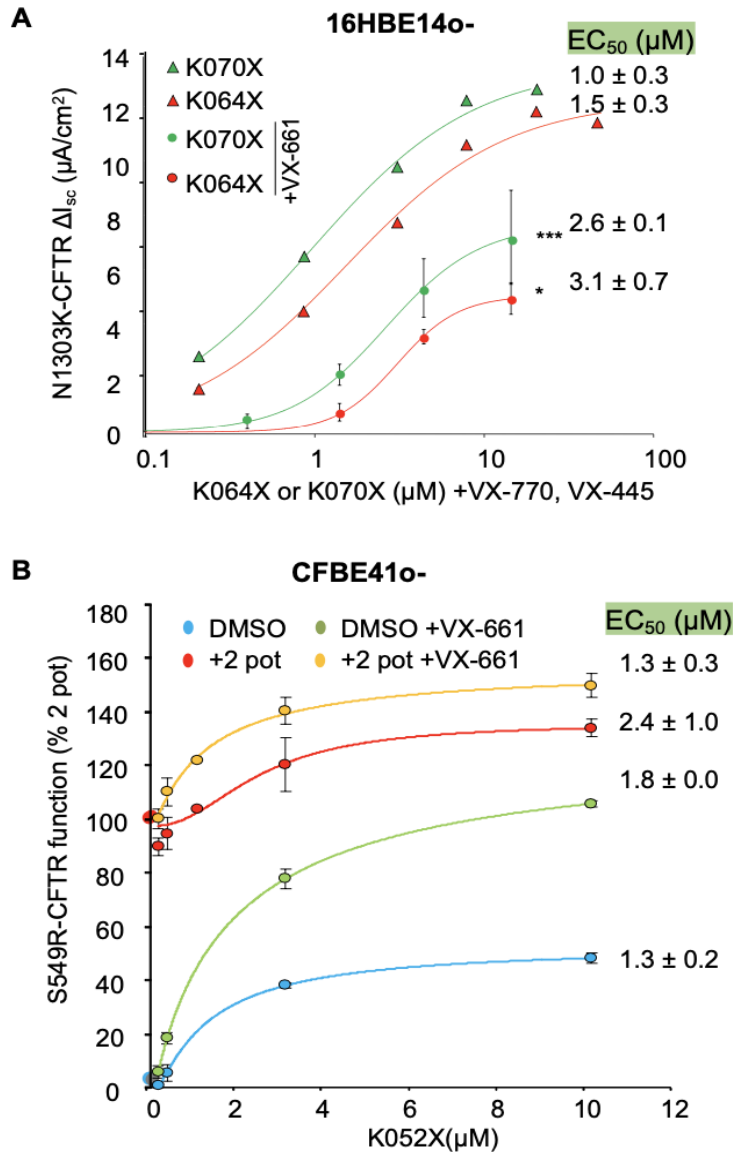


**Figure 4.10. Effect of VX-661 corrector on the potency of the K064X, K070X, and K052X potentiators on N1303K- and S549R-CFTR activity in 16HBE14o- and CFBE cells respectively, in the presence of the VX-770 and VX-445. A)** VX-661 treated (3 $\mu\text{M}$ , 24h) and non-treated 16less potent than cells not treated with VX-661 (n=1), when they are added as triple potentiation to 3  $\mu\text{M}$  VX-770 + 2  $\mu\text{M}$  VX-445, measured by short circuit current. The EC<sub>50</sub> values are shown. Data are means  $\pm$  SEM of three measurements. \* $P < 0.05$ , \*\* $P < 0.01$ , \*\*\* $P < 0.001$  by unpaired two-tailed t-test for the successive addition of potentiators. **B)** The dose-response of K052X in CFBE41o- S549R-CFTR cells in the presence or absence of 2 pot (VX-770+VX-445), with or without 3  $\mu\text{M}$  VX-661 treatment 24h. Data are means  $\pm$  SEM of three measurements.

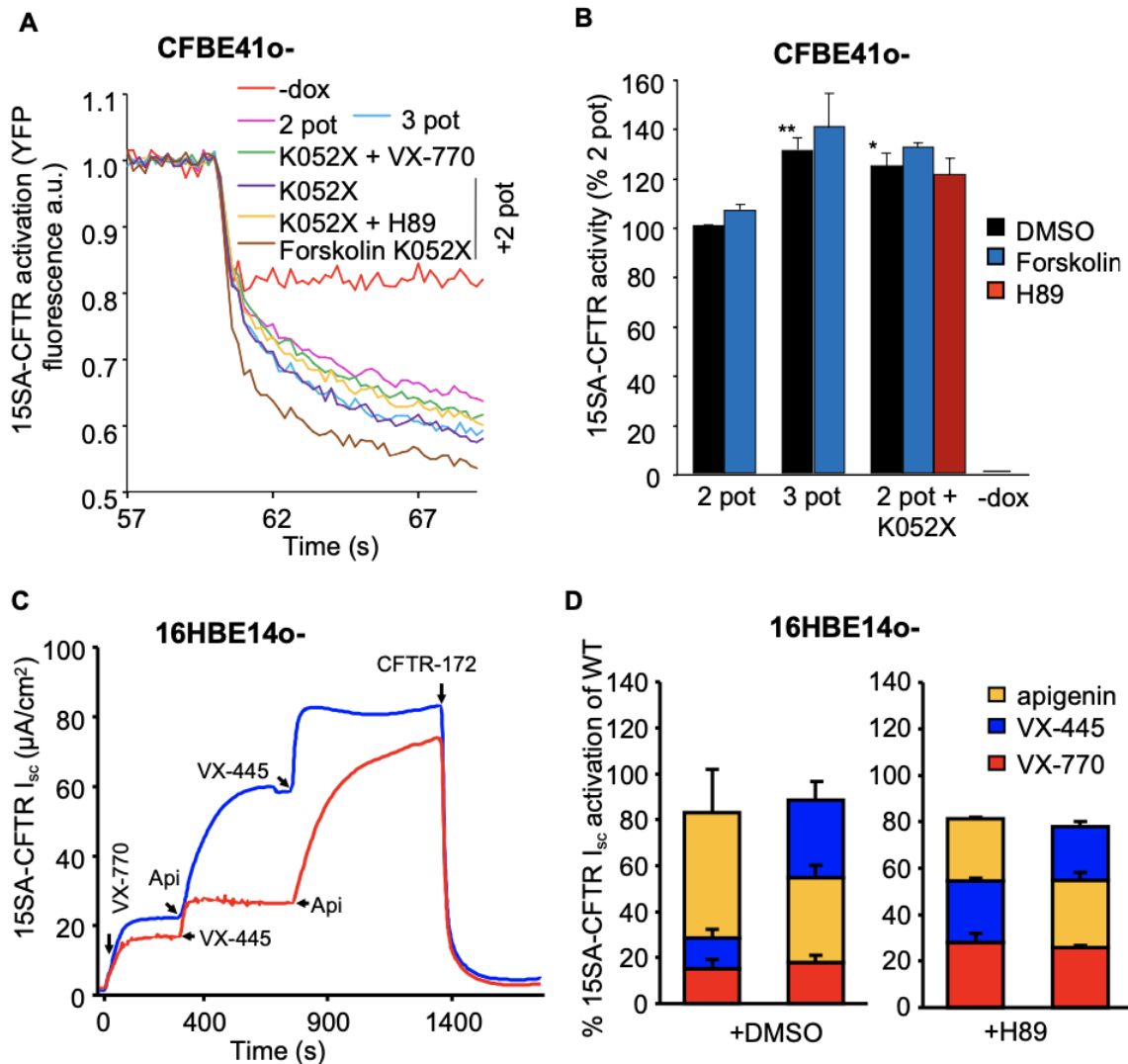


**Figure 4.11. Triple potentiator-mediated 15SA-CFTR activation does not require the CFTR R domain phosphorylation in CFBE41o- and 16HBEo- cells.** **A)** The time course of YFP fluorescence quenching was measured in CFBE41o- cells expressing the phosphorylation deficient 15SA-CFTR activity. Protein kinase A (PKA) was inhibited by 10 $\mu\text{M}$  H89 to suppress endogenous PKA activity. **B)** The VX-445 and VX-770 (2 pot) provoked forskolin-independent channel activity can be further augmented by the Class II Apigenin (3 pot) or K052X potentiator (means  $\pm$  SEM of three independent experiments,  $n=4$  technical replicates). A potent inhibitor of PKA, H89 (EC<sub>50</sub> ~135 nM), was used to suppress the residual phosphorylation of CFTR. as a negative control (red column inhibition by 10 $\mu\text{M}$  H89). **C-D)**  $I_{sc}$  activation by triple potentiator combination (3  $\mu\text{M}$  VX-770, 2  $\mu\text{M}$  VX-445, and 50  $\mu\text{M}$  Apigenin) in the absence of PKA stimulation of 15SA-CFTR. Analog traces **(C)** and quantification of the Ussing chamber measurements as shown in panel D. The abbreviations are: 2 pot = 3  $\mu\text{M}$  VX-770, 2  $\mu\text{M}$  VX-445; 3 pot = 3  $\mu\text{M}$  VX-770, 2  $\mu\text{M}$  VX-445, and 50  $\mu\text{M}$  Apigenin; -dox = no doxycycline; Forskolin at 20  $\mu\text{M}$  concentration. Data are means  $\pm$  SEM of three independent experiments,  $n=4$  technical replicates. \* $P < 0.05$ , \*\* $P < 0.01$ , \*\*\* $P < 0.001$  by unpaired two-tailed t-test.

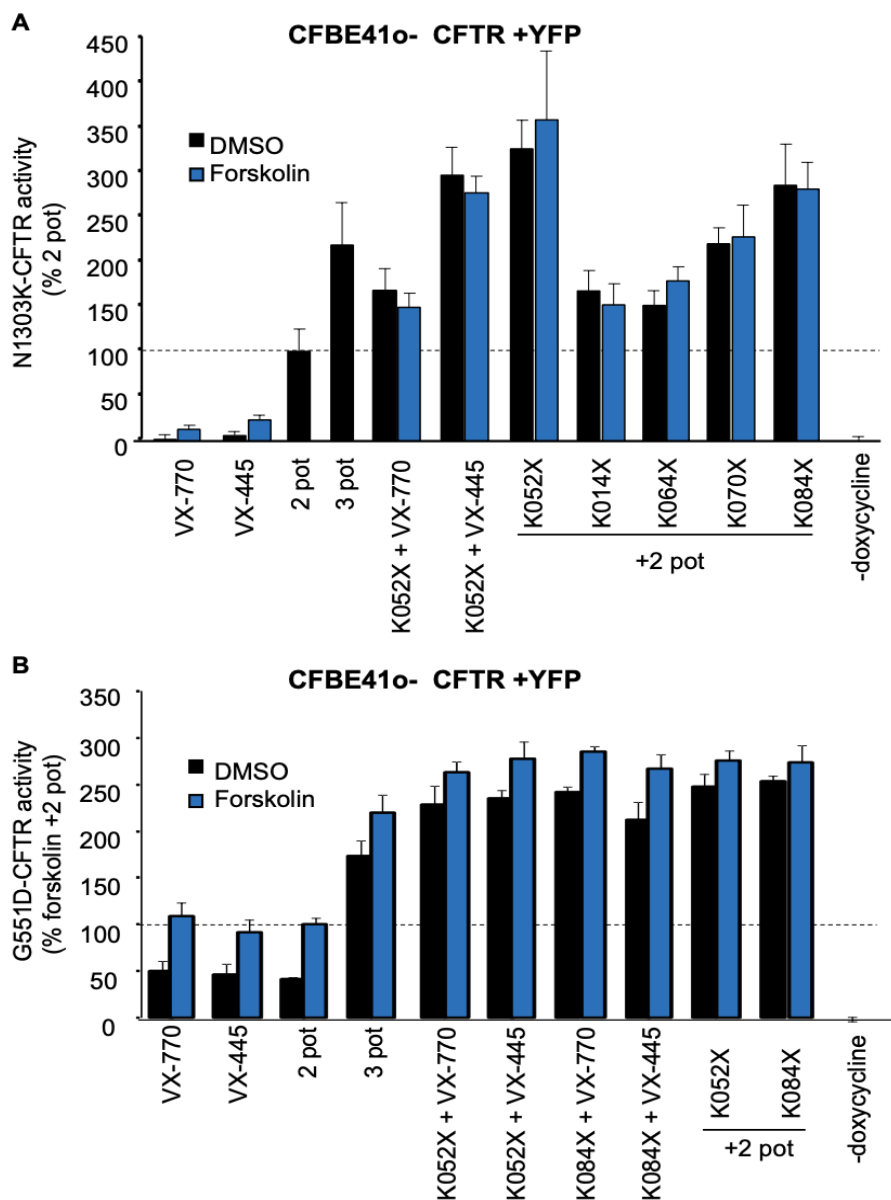


**Figure 4.12. Phosphorylation independency of K series compound on CFTR potentiation.** **A)** CFBE41o- N1303K-CFTR cells were 24h treated with 3 $\mu$ M VX-661 (n=1, technical replicates n=3-4). **B)** CFBE41o- G551D-CFTR cells (n=1, technical replicates n=3-4). Abbreviates: 2 pot= 3  $\mu$ M VX-770, 2  $\mu$ M VX-445; 3 pot= 2 pot + 50  $\mu$ M Apigenin.

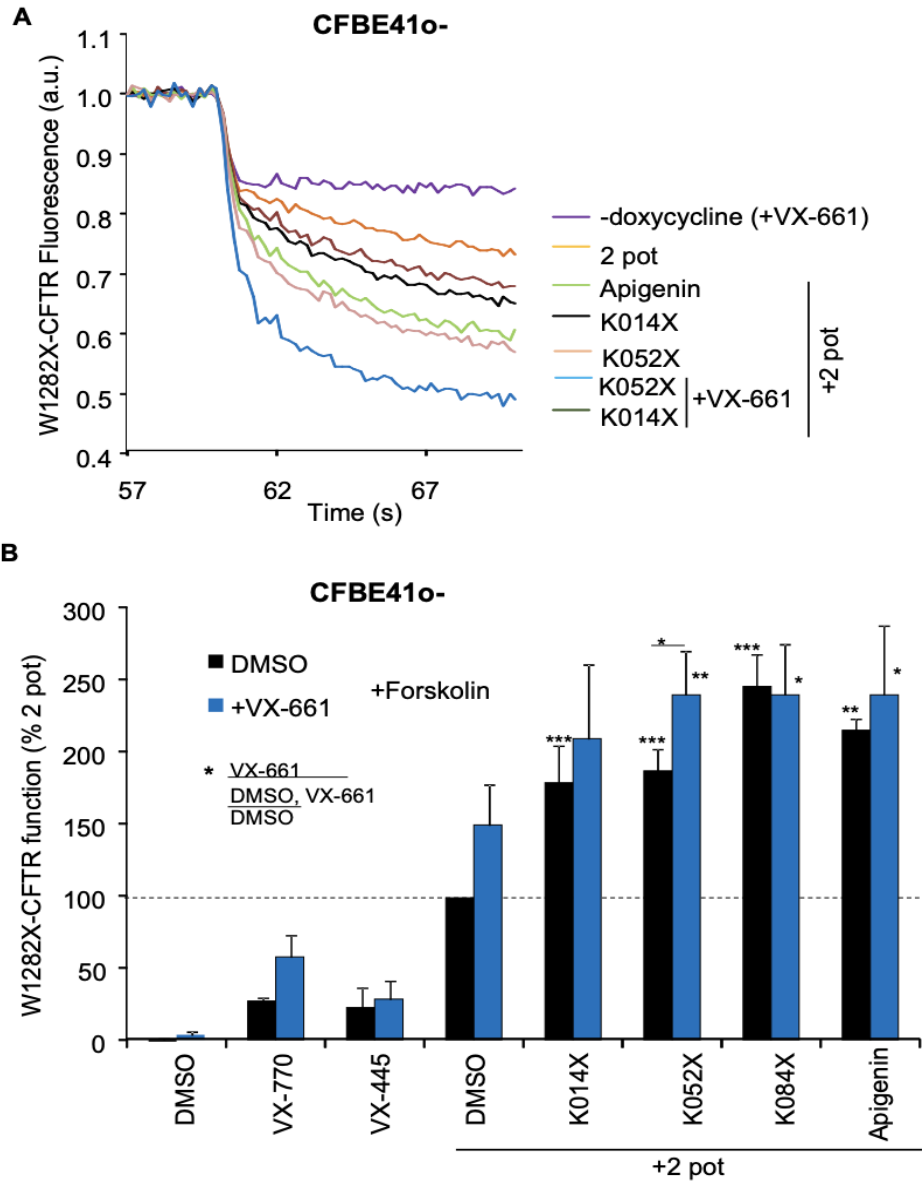


**Figure 4.13. Triple potentiator-mediated CFTR activation is independent of NBD-dimerization. A)** CFBE41o- W1282X-CFTR YFP assay (1h 3  $\mu$ M VX-661 treated at 37°C). **B)** Quantitative representation of CFTR function in CFBE41o- W1282X, expressed in percent of 2 pot (= 3 $\mu$ M VX-770 + 2 $\mu$ M VX-445). The blue columns show the CFTR function when the cells were corrected with VX-661 for 1hr at 32°C. Data are means  $\pm$  SEM of four measurements, n=3-4 technical measurements. \* $P$  < 0.05, \*\* $P$  < 0.01, \*\*\* $P$  < 0.001 by unpaired two-tailed t-test for the addition of potentiators.

## **Chapter 5: Discussion**

## **5.1 Characterization of novel co-potentiators of CFTR gating mutants as single, double, or triple potentiation**

Comprehensive preclinical and clinical research has shown that combinatorial pharmacotherapies, as opposed to monotherapies, are more effective in treating individual CFTR abnormalities [21, 83, 102]. Here, we show that the combination of three, structurally distinct potentiator combinations can to various degrees functionally rescue CFTR mutants with gating defects (G551D, N1303K, S549R/N, and W1282X) in stably transfected CFBE41o- and genetically engineered 16HBE14o- cell models. Besides the gating defect, some of these mutants also exhibit a folding defect (N1303K, S549R and W1282X) and a premature truncation codon which leads to the synthesis of a shortened protein as well as an RNA stability defect (W1282X), resulting in reduced PM expression. The majority of these mutations were incompletely corrected by the FDA-approved corrector-potentiator combination Trikafta.

Recently, we have discovered a novel CFTR corrector molecule, 4172, that has some activity acutely modulating the F508del CFTR channel function [79]. Analogs of 4172 exhibited potentiator activity for G551D-CFTR and mechanistically, exhibited similarities to previously identified co-potentiators, termed class-II potentiators according to a recently proposed classification scheme [83, 103, 104]. We assumed that 4172 analogs, as putative class II potentiators, might have a different mechanism of action (MOA) from the FDA-approved VX-770 (class I) and VX-445 (class III) potentiator combination (or 2 pot). From one of our collaborators, Dr. G. Marzaro (Pharmaceutical and Pharmacological Sciences, Padua University), we obtained a series of 4172 analog molecules. We set out to define and rank order a panel of 4172 small molecule analogs' efficacy and potency as co-potentiators to choose the best modulator and assess their effectiveness in CFTR functional rescue.

To enhance the functional rescue of G551D-CFTR and N1303K-CFTR CF mutants, our study sought to characterize 4172 analogs as co-potentiators with VX-770 or VX-445. The hypothesis was tested using transfected human bronchial epithelial cells (CFBE41o-) harboring

either the gating mutant G551D CFTR or the severe folding and gating mutation N1303K-CFTR, both of which were shown to be sensitive to VX-770 + co-potentiator combinations [41, 86]. However, the combination of co-potentiators + VX-445 has not been investigated yet. The CFTR function could be semi-quantitatively detected using the medium-throughput halide-sensitive YFP quenching assay with the cell lines co-expressing the CFTR variant and the halide-sensitive YFP. The compounds were evaluated at a concentration of 10  $\mu$ M, with saturating concentrations of either VX-770 (3  $\mu$ M) or VX-445 (2  $\mu$ M) (Figure 4.1). The VX-661 corrector (3  $\mu$ M, 24h, 37°C) was administered to cells that expressed N1303K-CFTR before the assay. 6 hit compounds were identified for G551D-CFTR (K014, 52, 64, 70, 71, 84X), while 9 analogs were selected for N1303K-CFTR (K014, 52, 53, 61, 62, 64, 70, 71, 73X). The K014, 52, 64, 70, and 71X compounds represent common hits for both mutations. The most effective compounds were selected for additional testing. The N1303K-CFTR has a different responsiveness to co-potentiators than G551D-CFTR, which is observed in the overall efficacy of double and triple potentiation.

This study expanded on previous research on CFTR modulators, also known as co-potentiators, which function in concert with VX-770 to raise channel activity of N1303K-CFTR and G551D-CFTR by approximately ~8- and ~1.5-fold, respectively, in comparison to VX-770 alone potentiation [41]. Here, novel co-potentiators such as K052X, K064X, and K071X with  $EC_{50}$  ranging from 0.75-28  $\mu$ M were found using high-throughput screening and short-circuit current measurements. Importantly, these scaffolds not only worked in concert with VX-770 but also with class III potentiator VX-445, to boost CFTR current. We prioritized the most effective 4172 analogs in combination with VX-770 or VX-445 based on their potency. K014X and K052X were found to be the most efficacious in combination with VX-770 and VX-445. Compounds K071X, K070X, and K064X were the most potent compounds. Evaluation of the effects of VX-770 and VX-445 on the potency of 4172 analogs found that the presence of either compound reduced the potency of K014X and K052X, but not of K064X, K070X, or K071X. This suggests that conformational changes caused by the binding of VX-770 or VX-445 may alter the binding site of

4172 analogs, thus affecting the potency of some compounds. Furthermore, differences in the efficacy and potency of 4172 analogs between G551D- and N1303K-CFTR may suggest a moderate level of mutation-specificity.

Veit. G., et al. [63] demonstrated that the potentiator efficacy of VX-445 is increased by the presence of VX-770, suggesting distinct binding sites for both compounds, which, however, are allosterically coupled. This is consistent with the distinct binding sites for VX-770 and VX-445 in the TMD1 and at the TMD1/2 interface, identified by cryo-EM [74, 100, 105, 106] and the recently demonstrated allosteric domain-domain coupling demonstrated at the backbone conformational dynamics of purified CFTR by hydrogen-deuterium exchange and by in silico molecular dynamics [77]. In a previous publication from our laboratory, Veit. G., et al demonstrated that potentiator compounds could be mechanistically grouped, using combinatorial profiling and average linkage analysis [107]. Pairwise administration of potentiators showed the additivity of the class II potentiator (e.g., Apigenin) with both VX-770 (class I) and VX-445. This warranted the introduction of a novel mechanistic potentiator class III to describe the distinct mechanism of VX-445. This inference was further supported by the additivity of all three potentiator classes for the potentiation of F508del and G551D CFTR [63]. The major limitation of apigenin, however, is its low potency and poor bioavailability [108]. Therefore, the 4172 analogs were interrogated for their ability to increase the functional correction of gating mutants in combination with VX-770+VX-445 (2 pot). Measurement of the potentiator function of the K014X analog of 4172 for G551D-CFTR in 16HBE by measuring short circuit current ( $I_{sc}$ ) in the Ussing chamber setup showed additivity of all three potentiators, which reached approximately  $50 \mu A/cm^2$ , corresponding to ~85% of the forskolin-activated WT-CFTR channel. In addition, K014X increased the efficacy of 2 pot combination on activation of the phosphorylated CFBE41o- G551D-CFTR. However, the effect of a third potentiator addition was only modest, likely because the G551D CFTR is already well (> 50% of the WT) potentiated by the VX-770+VX-445 combination.

In contrast, the N1303K CFTR mutant is only poorly responsive to VX-770 alone, and a combination of VX-770+VX-445 resulted in a functional correction of ~40% of the WT channel activity in 16HBE cells. The addition of 4172 analogs further enhanced the channel function by 18-26% of the WT current, reaching 60-80% of the WT current in N1303K-CFTR 16HBE14o- (Figure 4.7). The EC<sub>50</sub> of the 4172 analogs K014X, K052X, K064X, K070X and K084X for potentiating N1303K-CFTR was ~0.75-3.1 μM, which is a > 10-fold improvement in the potency in comparison to apigenin. We also demonstrated the potential of 4172 analogs in enhancing the functional correction of the N1303K-CFTR channel in human nasal epithelia (HNE) obtained from a patient homozygous for the N1303K mutation. In HNE cells, the VX-770+VX-445 combination produced a channel function that was approximately 20% of the WT current (Figure 4.8). The addition of 4172 analogs increased the N1303K function by > 10% of the WT current.

To investigate the utility of 4172 analogs as third potentiators their efficacy was tested for the additional mutants S549R-, S549N- and W1282X-CFTR. The S549R-CFTR mutant exhibits both a folding and gating defect and was therefore treated with the corrector VX-661. The triple potentiation with 2 pot + 4172 analogs significantly increased the channel function of S549R-CFTR compared to 2 pot. In contrast, the S549N-CFTR mutant was not responsive to the addition of 4172 analogs as third potentiators. The S549N mutation is highly responsive to class I and class III potentiators, in which the fractional benefit of a class II potentiator, conceivably targeted to a distinct binding site diminishing, which could explain the low responsiveness of S549N-CFTR to co-potentiation with 4172 analogs. In addition, we tested a novel combinatorial CFTR modulator effect in the functional rescue of the truncated CFTR variant, W1282X-CFTR. When treated with 10 μM K084X +2 pot, the W1282X-CFTR activity was 2.5-fold improved compared to that of the 2 pot.

In summary, we showed that five compounds could significantly improve the potentiation of the phosphorylated G551D-, N1303K-, S549R-, and W1282X-CFTR additively with both VX-770 and VX-445 out of the selected 72 pyrazole-pyrimidine compound library. These novel

compounds have a >10-fold higher potency than the investigational co-potentiator apigenin and a significantly increased potentiation efficacy in comparison to VX-770+VX-445 (2 pot) alone, and are excellent candidates for drug development. We could show the efficacy of pyrazole-pyrimidine compounds for mutations associated with only a gating defect (G551D), with a gating and folding defect (N1303K and S549R), as well as mutations with a gating, folding and synthesis defect (W1282X), suggesting the broad applicability of this drug strategy. Thus, the introduction of these compounds as a third potentiator has the potential to provide substantial additional benefits for patients with low to moderate responsiveness to established CFTR modulator drugs.

## **5.2 Towards mechanistic understanding of novel potentiators**

Investigating novel potentiators' interactions with the mutant CFTR protein can enhance cystic fibrosis treatments, focusing on binding locations and interactions. This knowledge can guide drug design and clarify CFTR activity regulation.

The detailed molecular mechanism of CFTR channel potentiation has only been partially uncovered. The binding site of VX-770 in the MSD1/MSD2 of CFTR was identified by cryo-EM [105] and confirmed by biochemical and electrophysiological assays [109, 110]. The VX-770-mediated CFTR activation was shown to be independent of ATP hydrolysis and NBD dimerization [46, 64, 111]. Similarly, the binding site of VX-445 has been identified in WT- and G551D-CFTR and validated by mutagenesis for its corrector and potentiator activities [112, 113].

To understand how phosphorylation affects the potentiator function of 4172 analogs, assays were conducted using the 15SA-CFTR variant, which lacks most of the PKA consensus phosphorylation sites. Using this mutant, we could show that the cumulative gating activation by VX-770, VX-445, and 4172 analogs does not depend on the PKA-mediated phosphorylation of the R-domain, reaching  $I_{sc}$  magnitudes similar to that recorded for the phosphorylated WT-CFTR. To further validate these results, the phosphorylation dependence of 4172 analogs in combination with VX-770+VX-445 was tested in other mutations such as G551D- and N1303K-CFTR.

Forskolin-mediated phosphorylation did not significantly change the triple potentiator-initiated channel activity.

Next, we tested whether triple potentiation by VX-770+VX-445 and 4172 analogs are NBD-dimerization dependent, using the W1282X-CFTR mutant that lacks most of its NBD2 domain. The results showed a significant improvement in the functional rescue of phosphorylated W1282X-CFTR activity by triple potentiation compared to the VX-770+VX-445 combination alone. The difference between rescued W1282X-CFTR with 3  $\mu$ M VX-661 and no correction (DMSO) was insignificant. Taken together, these results suggest that the triple-potentiator combination can bypass the canonical CFTR activation steps and lead to direct pore opening without R-domain phosphorylation and NBD dimerization.

We also attempted to determine whether there are interactions between modulator binding sites. Based on the VX-770 and VX-445 relatively high affinity to and distinct binding sites on the purified CFTR channel, it is plausible that these drugs do not compete for binding [105, 112, 113]. However, the presence of VX-770 did increase the efficacy of VX-445 as a potentiator, measured by the stimulated  $I_{sc}$  of G551D- and F508del-CFTR [63]. Conversely, the presence of VX-770 or VX-445 decreased the potency of some of the 4172 analogs (Figure 4.2). We also tested the impact of the correction of CFTR folding mutations on the efficacy and potency of 4172 analog potentiators. The results showed that in cells treated with 3  $\mu$ M VX-661, the 4172 analogs were less potent than in the absence of VX-661 correction, as assessed by short-circuit current measurements. The efficacy of K compound potentiation was also reduced in the VX-661 correction condition (Figure 4.11). These results suggest that structural rearrangements intervened by VX-770, VX-445 or VX-661 binding mediate allosteric changes in the configuration/dynamics of the 4172 analogs' binding site. While the binding site for 4172 analogs remains to be determined, the relative independence of 4172 analogs' potentiation from R-domain phosphorylation and NBD dimerization as well as the allosteric cross-talk with VX-770, VX-445 and VX-661, which all bind in the transmembrane domains of CFTR, may suggest that the 4172

analogs bind within the TMDs as well and reduce the activation energy of the open state and/or destabilize the closed state folding energy. Knowledge of the binding site would allow for structure-based optimization of these potentiator compounds, as recently accomplished for VX-770 [114].

In summary, we provided evidence demonstrating that the functional defect of some of the CF-causing mutations can be substantially augmented by novel class II potentiators, analogs of the 4172 compound, which is beyond the maximal activation elicited by the combination of Class I and III potentiators. We also showed that the combination of co-potentiators stimulated CFTR activation can bypass the canonical channel activation process, a phenomenon that raises some intriguing possibilities regarding their mechanism of action. The translational significance of our work stems from the possibility that the triple potentiation may offer a considerable improvement in rescuing the functional defect of certain rare CF mutations that presently lack FDA-approved drug therapy.

## References

1. ANDERSEN, D.H., *Cystic fibrosis of the pancreas and its relation to celiac disease - A clinical and pathologic study*, M.D. ANDERSEN, Editor. 1938: Am J Dis Child. p. 344–399.
2. SHWACHMAN, H., et al., *THE SYNDROME OF PANCREATIC INSUFFICIENCY AND BONE MARROW DYSFUNCTION*. J Pediatr, 1964. **65**: p. 645-63.
3. Riordan, J.R., et al., *Identification of the cystic fibrosis gene: cloning and characterization of complementary DNA*. Science, 1989. **245**(4922): p. 1066-73.
4. CFTR2 Database, C. Date last accessed October 27, 2023. <http://www.cftr2.org>
5. Cystic Fibrosis Mutation Database. Date last accessed October 20, 2023. <http://genet.sickkids.on.ca/>
6. Riordan, J.R., *CFTR function and prospects for therapy*. Annu Rev Biochem, 2008. **77**: p. 701-26.
7. Sockrider, M.M. and T.W. Ferkol, *Twenty facts about cystic fibrosis*. 2017, Am. J. Respir. Crit. Care Med. p. 23-24.
8. Gallego, Á., et al., *Congenital bilateral absence of the vas deferens (CBAVD): do genetic disorders modify assisted reproductive technologies outcomes?* Arch Esp Urol, 2019. **72**(10): p. 1038-1042.
9. Hanssens, L.S., J. Duchateau, and G.J. Casimir, *CFTR Protein: Not Just a Chloride Channel?* Cells, 2021. **10**(11).
10. Quinton, P.M., *The neglected ion: HCO<sub>3</sub><sup>-</sup>*. Nat Med, 2001. **7**(3): p. 292-3.
11. Khan, T.Z., et al., *Early pulmonary inflammation in infants with cystic fibrosis*. Am J Respir Crit Care Med, 1995. **151**(4): p. 1075-82.
12. Rosen, B.H., et al., *Infection Is Not Required for Mucoinflammatory Lung Disease in CFTR-Knockout Ferrets*. Am J Respir Crit Care Med, 2018. **197**(10): p. 1308-1318.
13. Balazs, A. and M.A. Mall, *Mucus obstruction and inflammation in early cystic fibrosis lung disease: Emerging role of the IL-1 signaling pathway*. Pediatr Pulmonol, 2019. **54 Suppl 3**: p. S5-S12.
14. Roesch, E.A., D.P. Nichols, and J.F. Chmiel, *Inflammation in cystic fibrosis: An update*. Pediatr Pulmonol, 2018. **53**(S3): p. S30-S50.
15. Ideozu, J.E., et al., *Transcriptome Profiling and Molecular Therapeutic Advances in Cystic Fibrosis: Recent Insights*. Genes (Basel), 2019. **10**(3).
16. Meyerholz, D.K., et al., *Lack of cystic fibrosis transmembrane conductance regulator disrupts fetal airway development in pigs*. Lab Invest, 2018. **98**(6): p. 825-838.

17. Meyerholz, D.K., et al., *Loss of cystic fibrosis transmembrane conductance regulator function produces abnormalities in tracheal development in neonatal pigs and young children*. Am J Respir Crit Care Med, 2010. **182**(10): p. 1251-61.
18. Adam, R.J., et al., *Air trapping and airflow obstruction in newborn cystic fibrosis piglets*. Am J Respir Crit Care Med, 2013. **188**(12): p. 1434-41.
19. Stoltz, D.A., D.K. Meyerholz, and M.J. Welsh, *Origins of cystic fibrosis lung disease*. N Engl J Med, 2015. **372**(4): p. 351-62.
20. Hwang, T.C., et al., *Structure basis of CFTR folding, function and pharmacology*. J Cyst Fibros, 2023. **22 Suppl 1**: p. S5-S11.
21. Veit, G., et al., *From CFTR biology toward combinatorial pharmacotherapy: expanded classification of cystic fibrosis mutations*. Mol Biol Cell, 2016. **27**(3): p. 424-33.
22. Cheng, S.H., et al., *Defective intracellular transport and processing of CFTR is the molecular basis of most cystic fibrosis*. Cell, 1990. **63**(4): p. 827-34.
23. Ward, C.L., S. Omura, and R.R. Kopito, *Degradation of CFTR by the ubiquitin-proteasome pathway*. Cell, 1995. **83**(1): p. 121-7.
24. Amaral, M.D. and C.M. Farinha, *Rescuing mutant CFTR: a multi-task approach to a better outcome in treating cystic fibrosis*. Curr Pharm Des, 2013. **19**(19): p. 3497-508.
25. Balch, W.E., D.M. Roth, and D.M. Hutt, *Emergent properties of proteostasis in managing cystic fibrosis*. Cold Spring Harb Perspect Biol, 2011. **3**(2).
26. Wang, W., et al., *G551D mutation impairs PKA-dependent activation of CFTR channel that can be restored by novel GOF mutations*. Am J Physiol Lung Cell Mol Physiol, 2020. **319**(5): p. L770-L785.
27. Derand, R., L. Bulteau-Pignoux, and F. Becq, *The cystic fibrosis mutation G551D alters the non-Michaelis-Menten behavior of the cystic fibrosis transmembrane conductance regulator (CFTR) channel and abolishes the inhibitory Genistein binding site*. J Biol Chem, 2002. **277**(39): p. 35999-6004.
28. *Patient registry: 2008 annual data report to the Center directors*. 2009: Cystic Fibrosis Foundation.
29. McKone, E.F., et al., *Effect of genotype on phenotype and mortality in cystic fibrosis: a retrospective cohort study*. Lancet, 2003. **361**(9370): p. 1671-6.
30. Osborne, L., et al., *Incidence and expression of the N1303K mutation of the cystic fibrosis (CFTR) gene*. Hum Genet, 1992. **89**(6): p. 653-8.
31. Du, K. and G.L. Lukacs, *Cooperative assembly and misfolding of CFTR domains in vivo*. Mol Biol Cell, 2009. **20**(7): p. 1903-15.

32. Csanády, L., P. Vergani, and D.C. Gadsby, *Strict coupling between CFTR's catalytic cycle and gating of its Cl<sup>-</sup> ion pore revealed by distributions of open channel burst durations*. Proc Natl Acad Sci U S A, 2010. **107**(3): p. 1241-6.
33. Hwang, T.C., et al., *Structural mechanisms of CFTR function and dysfunction*. J Gen Physiol, 2018. **150**(4): p. 539-570.
34. Berger, A.L., et al., *Mutations that change the position of the putative gamma-phosphate linker in the nucleotide binding domains of CFTR alter channel gating*. J Biol Chem, 2002. **277**(3): p. 2125-31.
35. DeStefano, S., M. Gees, and T.C. Hwang, *Physiological and pharmacological characterization of the N1303K mutant CFTR*. J Cyst Fibros, 2018. **17**(5): p. 573-581.
36. Watson, M.S., et al., *Cystic fibrosis population carrier screening: 2004 revision of American College of Medical Genetics mutation panel*. Genet Med, 2004. **6**(5): p. 387-91.
37. Haggie, P.M., et al., *Correctors and Potentiators Rescue Function of the Truncated W1282X-Cystic Fibrosis Transmembrane Regulator (CFTR) Translation Product*. J Biol Chem, 2017. **292**(3): p. 771-785.
38. Kirk, K.L. and W. Wang, *A unified view of cystic fibrosis transmembrane conductance regulator (CFTR) gating: combining the allostereism of a ligand-gated channel with the enzymatic activity of an ATP-binding cassette (ABC) transporter*. J Biol Chem, 2011. **286**(15): p. 12813-9.
39. Wang, W., et al., *Robust Stimulation of W1282X-CFTR Channel Activity by a Combination of Allosteric Modulators*. PLoS One, 2016. **11**(3): p. e0152232.
40. Rowe, S.M., et al., *Suppression of CFTR premature termination codons and rescue of CFTR protein and function by the synthetic aminoglycoside NB54*. J Mol Med (Berl), 2011. **89**(11): p. 1149-61.
41. Phuan, P.W., et al., *Combination potentiator ('co-potentiator') therapy for CF caused by CFTR mutants, including N1303K, that are poorly responsive to single potentiators*. J Cyst Fibros, 2018. **17**(5): p. 595-606.
42. Dawson, K.P. and P.M. Frossard, *The S549R (T-->G) cystic fibrosis gene mutation*. J Trop Pediatr, 2001. **47**(4): p. 196-8.
43. Ma, J., et al., *Function of the R domain in the cystic fibrosis transmembrane conductance regulator chloride channel*. J Biol Chem, 1997. **272**(44): p. 28133-41.
44. Chappe, V., et al., *Phosphorylation of protein kinase C sites in NBD1 and the R domain control CFTR channel activation by PKA*. J Physiol, 2003. **548**(Pt 1): p. 39-52.
45. Billet, A., et al., *Regulation of the cystic fibrosis transmembrane conductance regulator anion channel by tyrosine phosphorylation*. FASEB J, 2015. **29**(9): p. 3945-53.

46. Jih, K.Y. and T.C. Hwang, *Vx-770 potentiates CFTR function by promoting decoupling between the gating cycle and ATP hydrolysis cycle*. Proc Natl Acad Sci U S A, 2013. **110**(11): p. 4404-9.
47. Nguyen, J.P., et al., *Modulation of cAMP metabolism for CFTR potentiation in human airway epithelial cells*. Sci Rep, 2021. **11**(1): p. 904.
48. Hwang, T.C. and D.N. Sheppard, *Gating of the CFTR Cl<sup>-</sup> channel by ATP-driven nucleotide-binding domain dimerisation*. J Physiol, 2009. **587**(Pt 10): p. 2151-61.
49. Hwang, T.C. and K.L. Kirk, *The CFTR ion channel: gating, regulation, and anion permeation*. Cold Spring Harb Perspect Med, 2013. **3**(1): p. a009498.
50. Chappe, V., et al., *Stimulatory and inhibitory protein kinase C consensus sequences regulate the cystic fibrosis transmembrane conductance regulator*. Proc Natl Acad Sci U S A, 2004. **101**(1): p. 390-5.
51. Zhang, Z., F. Liu, and J. Chen, *Molecular structure of the ATP-bound, phosphorylated human CFTR*. Proc Natl Acad Sci U S A, 2018. **115**(50): p. 12757-12762.
52. ter Beek, J., A. Guskov, and D.J. Slotboom, *Structural diversity of ABC transporters*. J Gen Physiol, 2014. **143**(4): p. 419-35.
53. Chappe, V., et al., *Phosphorylation of CFTR by PKA promotes binding of the regulatory domain*. EMBO J, 2005. **24**(15): p. 2730-40.
54. Farkas, B., et al., *Discovering the chloride pathway in the CFTR channel*. Cell Mol Life Sci, 2020. **77**(4): p. 765-778.
55. Wang, W., B.C. Roessler, and K.L. Kirk, *An electrostatic interaction at the tetrahelix bundle promotes phosphorylation-dependent cystic fibrosis transmembrane conductance regulator (CFTR) channel opening*. J Biol Chem, 2014. **289**(44): p. 30364-78.
56. Weng, J.W., K.N. Fan, and W.N. Wang, *The conformational transition pathway of ATP binding cassette transporter MsbA revealed by atomistic simulations*. J Biol Chem, 2010. **285**(5): p. 3053-63.
57. Vergani, P., A.C. Nairn, and D.C. Gadsby, *On the mechanism of MgATP-dependent gating of CFTR Cl<sup>-</sup> channels*. J Gen Physiol, 2003. **121**(1): p. 17-36.
58. Van Goor, F., et al., *Rescue of CF airway epithelial cell function in vitro by a CFTR potentiator, VX-770*. Proc Natl Acad Sci U S A, 2009. **106**(44): p. 18825-30.
59. Wainwright, C.E., et al., *Lumacaftor-Ivacaftor in Patients with Cystic Fibrosis Homozygous for Phe508del CFTR*. N Engl J Med, 2015. **373**(3): p. 220-31.
60. Keating, D., et al., *VX-445-Tezacaftor-Ivacaftor in Patients with Cystic Fibrosis and One or Two Phe508del Alleles*. N Engl J Med, 2018. **379**(17): p. 1612-1620.

61. Ramsey, B.W., et al., *A CFTR potentiator in patients with cystic fibrosis and the G551D mutation*. N Engl J Med, 2011. **365**(18): p. 1663-72.
62. Shaughnessy, C.A., P.L. Zeitlin, and P.E. Bratcher, *Elexacaftor is a CFTR potentiator and acts synergistically with ivacaftor during acute and chronic treatment*. Sci Rep, 2021. **11**(1): p. 19810.
63. Veit, G., C. Vaccarin, and G.L. Lukacs, *Elexacaftor co-potentiates the activity of F508del and gating mutants of CFTR*. J Cyst Fibros, 2021. **20**(5): p. 895-898.
64. Eckford, P.D., et al., *Cystic fibrosis transmembrane conductance regulator (CFTR) potentiator VX-770 (ivacaftor) opens the defective channel gate of mutant CFTR in a phosphorylation-dependent but ATP-independent manner*. J Biol Chem, 2012. **287**(44): p. 36639-49.
65. Du, K., M. Sharma, and G.L. Lukacs, *The DeltaF508 cystic fibrosis mutation impairs domain-domain interactions and arrests post-translational folding of CFTR*. Nat Struct Mol Biol, 2005. **12**(1): p. 17-25.
66. He, L., et al., *Restoration of domain folding and interdomain assembly by second-site suppressors of the DeltaF508 mutation in CFTR*. FASEB J, 2010. **24**(8): p. 3103-12.
67. Serohijos, A.W., et al., *Diminished self-chaperoning activity of the DeltaF508 mutant of CFTR results in protein misfolding*. PLoS Comput Biol, 2008. **4**(2): p. e1000008.
68. Lukacs, G.L. and A.S. Verkman, *CFTR: folding, misfolding and correcting the DeltaF508 conformational defect*. Trends Mol Med, 2012. **18**(2): p. 81-91.
69. Mijnders, M., B. Kleizen, and I. Braakman, *Correcting CFTR folding defects by small-molecule correctors to cure cystic fibrosis*. Curr Opin Pharmacol, 2017. **34**: p. 83-90.
70. Ruffin, M., et al., *Vx-809/Vx-770 treatment reduces inflammatory response to Pseudomonas aeruginosa in primary differentiated cystic fibrosis bronchial epithelial cells*. Am J Physiol Lung Cell Mol Physiol, 2018. **314**(4): p. L635-L641.
71. in *Pharmacoeconomic Review Report: Lumacaftor/Ivacaftor (Orkambi): (Vertex Pharmaceuticals (Canada) Incorporated): Indication: For the treatment of cystic fibrosis in patients 6 years of age and older who are homozygous for the F508del mutation in the cystic fibrosis transmembrane conductance regulator gene*. 2018: Ottawa (ON).
72. Veit, G., et al., *Some gating potentiators, including VX-770, diminish  $\Delta$ F508-CFTR functional expression*. Sci Transl Med, 2014. **6**(246): p. 246ra97.
73. Avramescu, R.G., et al., *Mutation-specific downregulation of CFTR2 variants by gating potentiators*. Hum Mol Genet, 2017. **26**(24): p. 4873-4885.

74. Ren, H.Y., et al., *VX-809 corrects folding defects in cystic fibrosis transmembrane conductance regulator protein through action on membrane-spanning domain 1*. Mol Biol Cell, 2013. **24**(19): p. 3016-24.
75. Awatade, N.T., et al., *Measurements of Functional Responses in Human Primary Lung Cells as a Basis for Personalized Therapy for Cystic Fibrosis*. EBioMedicine, 2015. **2**(2): p. 147-53.
76. Pedemonte, N. and L.J. Galletta, *Pharmacological Correctors of Mutant CFTR Mistrafficking*. Front Pharmacol, 2012. **3**: p. 175.
77. Soya, N., et al., *Folding correctors can restore CFTR posttranslational folding landscape by allosteric domain-domain coupling*. Nat Commun, 2023. **14**(1): p. 6868.
78. Liu, F., et al., *Molecular Structure of the Human CFTR Ion Channel*. Cell, 2017. **169**(1): p. 85-95.e8.
79. Veit, G., et al., *Structure-guided combination therapy to potently improve the function of mutant CFTRs*. Nat Med, 2018. **24**(11): p. 1732-1742.
80. Caci, E., et al., *Evidence for direct CFTR inhibition by CFTR(inh)-172 based on Arg347 mutagenesis*. Biochem J, 2008. **413**(1): p. 135-42.
81. Lopes-Pacheco, M., *CFTR Modulators: Shedding Light on Precision Medicine for Cystic Fibrosis*. Front Pharmacol, 2016. **7**: p. 275.
82. Zhang, Z., F. Liu, and J. Chen, *Conformational Changes of CFTR upon Phosphorylation and ATP Binding*. Cell, 2017. **170**(3): p. 483-491.e8.
83. Veit, G., et al., *Mutation-specific dual potentiators maximize rescue of CFTR gating mutants*. J Cyst Fibros, 2020. **19**(2): p. 236-244.
84. Yeh, H.I., et al., *CFTR Modulators: From Mechanism to Targeted Therapeutics*. Handb Exp Pharmacol, 2022.
85. Fiedorczuk, K. and J. Chen, *Molecular structures reveal synergistic rescue of  $\Delta$ 508 CFTR by Trikafta modulators*. Science, 2022. **378**(6617): p. 284-290.
86. Veit, G., et al., *Allosteric folding correction of F508del and rare CFTR mutants by elexacaftor-tezacaftor-ivacaftor (Trikafta) combination*. JCI Insight, 2020. **5**(18).
87. Schroeder, J.A., et al., *The phosphodiesterase inhibitor isobutylmethylxanthine attenuates behavioral sensitization to cocaine*. Behav Pharmacol, 2012. **23**(3): p. 310-4.
88. Sharma, M., et al., *Misfolding diverts CFTR from recycling to degradation: quality control at early endosomes*. J Cell Biol, 2004. **164**(6): p. 923-33.
89. Veit, G., et al., *Proinflammatory cytokine secretion is suppressed by TMEM16A or CFTR channel activity in human cystic fibrosis bronchial epithelia*. Mol Biol Cell, 2012. **23**(21): p. 4188-202.

90. Okiyoneda, T., et al., *Mechanism-based corrector combination restores  $\Delta F508$ -CFTR folding and function*. Nat Chem Biol, 2013. **9**(7): p. 444-54.
91. Namkung, W., et al., *Inhibition of  $Ca^{2+}$ -activated  $Cl^-$  channels by gallotannins as a possible molecular basis for health benefits of red wine and green tea*. FASEB J, 2010. **24**(11): p. 4178-86.
92. Ehrhardt, C., et al., *Towards an in vitro model of cystic fibrosis small airway epithelium: characterisation of the human bronchial epithelial cell line CFBE41o*. Cell Tissue Res, 2006. **323**(3): p. 405-15.
93. Müller, L., et al., *Culturing of human nasal epithelial cells at the air liquid interface*. J Vis Exp, 2013(80).
94. Liu, X., et al., *ROCK inhibitor and feeder cells induce the conditional reprogramming of epithelial cells*. Am J Pathol, 2012. **180**(2): p. 599-607.
95. Neuberger, T., et al., *Use of primary cultures of human bronchial epithelial cells isolated from cystic fibrosis patients for the pre-clinical testing of CFTR modulators*. Methods Mol Biol, 2011. **741**: p. 39-54.
96. in *The Impact of Food Bioactives on Health: in vitro and ex vivo models*, K. Verhoeckx, et al., Editors. 2015: Cham (CH).
97. Lopez-Valdez, J.A., et al., *Cystic fibrosis: current concepts*. Bol Med Hosp Infant Mex, 2021. **78**(6): p. 584-596.
98. Valley, H.C., et al., *Isogenic cell models of cystic fibrosis-causing variants in natively expressing pulmonary epithelial cells*. J Cyst Fibros, 2019. **18**(4): p. 476-483.
99. release, V.p., accessed on 6 July 2021.
100. Fiedorczuk, K. and J. Chen, *Mechanism of CFTR correction by type I folding correctors*. Cell, 2022. **185**(1): p. 158-168.e11.
101. Schnúr, A., et al., *Phosphorylation-dependent modulation of CFTR macromolecular signalling complex activity by cigarette smoke condensate in airway epithelia*. Sci Rep, 2019. **9**(1): p. 12706.
102. Heijerman, H.G.M., et al., *Efficacy and safety of the elexacaftor plus tezacaftor plus ivacaftor combination regimen in people with cystic fibrosis homozygous for the F508del mutation: a double-blind, randomised, phase 3 trial*. Lancet, 2019. **394**(10212): p. 1940-1948.
103. Phuan, P.W., et al., *Nanomolar-potency 'co-potentiator' therapy for cystic fibrosis caused by a defined subset of minimal function CFTR mutants*. Sci Rep, 2019. **9**(1): p. 17640.
104. Bose, S.J., et al., *Towards next generation therapies for cystic fibrosis: Folding, function and pharmacology of CFTR*. J Cyst Fibros, 2020. **19 Suppl 1**: p. S25-S32.

105. Liu, F., et al., *Structural identification of a hotspot on CFTR for potentiation*. Science, 2019. **364**(6446): p. 1184-1188.
106. C., W., et al., *Mechanism of dual pharmacological correction and potentiation of human CFTR*. bioRxiv, 2022.
107. Kruger, T.F., et al., *The development of one- and two-cell mouse embryos in the absence of human serum*. S Afr Med J, 1986. **70**(9): p. 542-3.
108. Salehi, B., et al., *The Therapeutic Potential of Apigenin*. Int J Mol Sci, 2019. **20**(6).
109. Laselva, O., et al., *Identification of binding sites for ivacaftor on the cystic fibrosis transmembrane conductance regulator*. iScience, 2021. **24**(6): p. 102542.
110. Yeh, H.I., et al., *Identifying the molecular target sites for CFTR potentiators GLPG1837 and VX-770*. J Gen Physiol, 2019.
111. Yeh, H.I., et al., *A common mechanism for CFTR potentiators*. J Gen Physiol, 2017. **149**(12): p. 1105-1118.
112. Fiedorczuk, K. and J. Chen, *Molecular structures reveal synergistic rescue of Delta508 CFTR by Trikafta modulators*. Science, 2022. **378**(6617): p. 284-290.
113. Wang, C., et al., *Mechanism of dual pharmacological correction and potentiation of human CFTR*. bioRxiv, 2022: p. 2022.10.10.510913.
114. Liu, F., et al., *Structure-based discovery of CFTR potentiators and inhibitors*. bioRxiv, 2023.

## **Appendices**

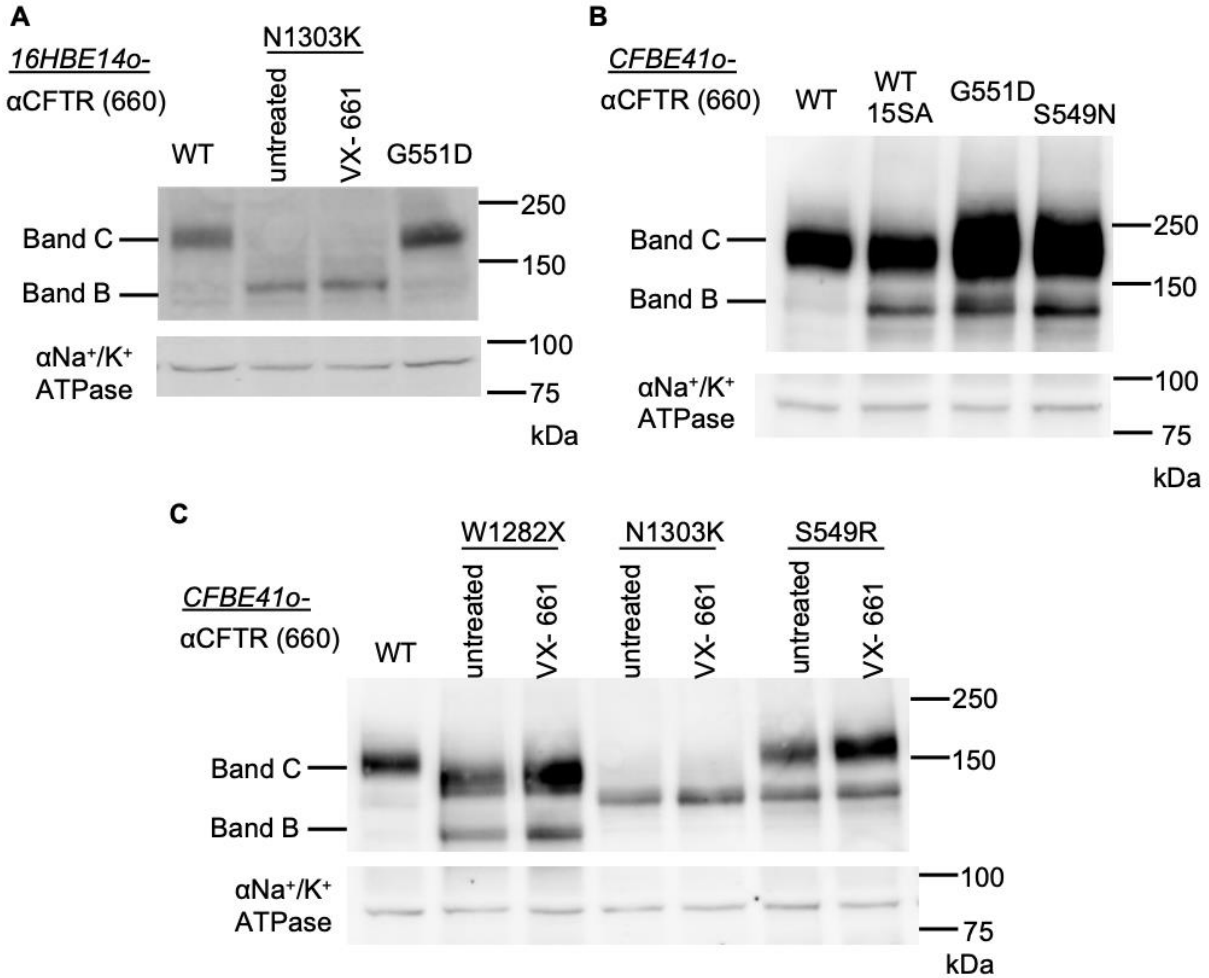


**Figure S.1. The CFTR expression of WT-, G551D-, and N1303K-, S549R-, S549N- and W1282X-CFTR.** The band C, which shows the complex-glycosylated or mature form of CFTR, is less in N1303K-CFTR than WT-CFTR but can be improved partially by the VX-661, as a CFTR corrector, while band B shows the immature form of CFTR. **A)** CFTR expression of single allele 16HBE14o- WT-, N1303K- and G551D-CFTR. **B)** CFTR expression of double allele CFBE41o- WT-, WT-15SA-, G551D-, and S549N-CFTR. **C)** CFTR expression of double allele CFBE41o- WT-, W1282X-, N1303K-, and S549R-CFTR, either treated with 3μM VX-661 for 24h, at 37°C (n=2).

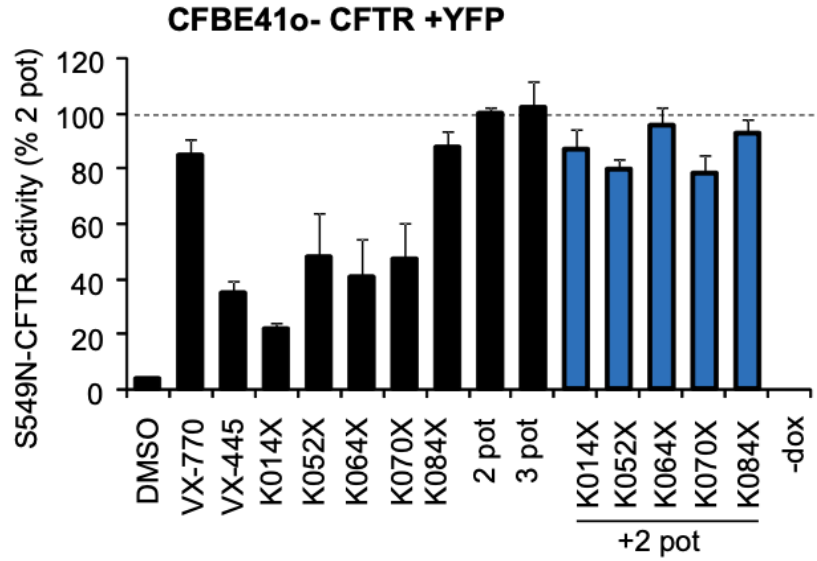


**Figure S.2. The combination of multiple potentiators does not lead to activation of S549N- CFTR/YFP.** Triple potentiation effects of analogs K014, 52, 64, 70, and 84X. The legend is described as: -dox= no doxycycline; 2  $\mu$ M VX-445; 3  $\mu$ M VX-770; 2 pot = VX-445+VX-770; 3 pot = 3  $\mu$ M VX-770+ 2  $\mu$ M VX-445 + 50  $\mu$ M Apigenin; and the triple combination of doses of K052X in addition to 2 pot (data are means  $\pm$  SEM of 3 independent experiment, 4 replicates per experiment). Cells were induced 4d with 250 ng/ml doxycycline at 37°C.